Level widths and level densities of nuclei in the $32 \leqslant A \leqslant 60$ mass region inferred from fluctuation analysis of total neutron cross sections

W. P. Abfalterer,[1] R. W. Finlay,[2] and S. M. Grimes[2]
[1]*Los Alamos National Laboratory, Los Alamos, New Mexico 87545*
[2]*Ohio University, Athens, Ohio 45701*
(Received 8 May 2000; published 17 November 2000)

Level widths and level densities of nuclei in the $32 \leqslant A \leqslant 60$ mass region are inferred from the fluctuation analysis of total neutron cross sections. The experimentally determined level densities are compared to phenomenological and microscopic predictions. The total neutron cross sections were measured in the $0.75 \leqslant E_n \leqslant 11.3$ MeV range for ^{31}P, ^{32}S, ^{39}K, ^{51}V, ^{56}Fe, and ^{59}Co using a white neutron source and standard time-of-flight techniques. Measured cross sections agree well in magnitude and structure with earlier measurements. Nuclear level widths and cross section variances were determined for the compound nuclei ^{32}P, ^{33}S, ^{40}K, ^{52}V, ^{57}Fe, and ^{60}Co by means of Fourier analysis of the fluctuating excitation functions and subsequent least squares fit to the resulting $\ln S_k$ spectra. Nuclear level densities for the above compound nuclei were extracted by relating them to the variance (variance method) of the total neutron cross sections via Ericson theory of fluctuating cross sections. Furthermore, level density values were derived by relating level densities to average level widths (gamma method) via compound nuclear theory. The present study shows good agreement between the two methods for ^{32}P and ^{33}S, with an uncertainty of 30–40 %. Inclusion of a finite energy resolution correction and use of local instead of global optical model parameters improve agreement, but do not resolve the discrepancy between the two methods completely, especially for $A > 40$. Nuclear level densities were compared with microscopic calculations utilizing a BCS pairing Hamiltonian and specific sets of realistic sets of single-particle energies. A further comparison was made with results obtained from phenomenological models based on the Fermi gas formalism. For ^{32}P, ^{33}S, and ^{40}K, experimental values and phenomenological predictions agree well, but diverge with increasing A. From least squares fits to the present level density data, level density parameters (a and Δ) were extracted for ^{32}P, ^{33}S, and ^{40}K. Results for the level density parameter are consistent with $a = A/9$.

PACS number(s): 21.10.Ma, 28.20.Cz, 25.40.−h

I. INTRODUCTION

A considerable number of phenomena related to the formation and decay of a compound nucleus system can be described in terms of the statistical theory of nuclear reactions. Absorption of the incident particle by the target leads to the formation of a so-called ''compound nucleus.'' The resulting system reaches equilibrium and eventually decays to various states independent of the entrance channel. The decay is governed by the density of final states ρ_f, and the matrix element between the initial state i and the final state f, as expressed by Fermi's golden rule

$$w = \frac{2\pi}{\hbar} |H_{if}|^2 \rho_f , \tag{1.1}$$

where w is the transition probability.

The formalism developed by Hauser and Feshbach [1], based upon Fermi's golden rule, allows the calculation of reaction cross sections; the nuclear level density together with a given set of integrals of motion uniquely characterizes the nucleus and the given process. Therefore an accurate knowledge of level densities cannot only predict otherwise inaccessible reaction cross sections, but also help in the understanding of the reaction mechanisms themselves.

Unfortunately almost 60 years of substantial effort in both theoretical and experimental work on nuclear level densities does not allow reliable calculation of missing level density data, especially at excitation energies above 10 MeV and for nuclei away from the stability line [2].

For instance, reliable nuclear level density data are of great importance in the design and operation of fission reactors. In particular they are needed to calculate the fission cross sections of the fuel and the fission products reliably, and therefore allow a prediction of the neutronic performance of the reactor after fission product buildup.

In the case of fusion reactors, knowledge of the interaction of massive amounts of 14 MeV neutrons with the structural and blanket material is essential, interaction with the fuel being minimal in this case.

A third application of nuclear level densities is in the calculation of nuclear reactions in astrophysical systems, spanning a wide range in time scale, temperature, and elemental composition, very often inaccessible to experimental techniques.

The current progress in nuclear level density theories and experiments is well described in an IAEA conference report [3].

Besides Grimes' method [4–6] in which he measured for (p,n) and (α,n) reactions the total cross section for the population of all levels below the neutron binding energy, and then derived level density information by means of a Hauser-Feshbach fit to the cross sections, fluctuation analysis of excitation functions is the only presently known alternate direct method for deriving level density information at excitation energies beyond 10 MeV. Up to now level widths have

been measured by fluctuation analysis of excitation functions, mostly for (p,α) or (p,p) reactions, for a large number of nuclei in the mass range $A=20-60$, mostly for excitation energies around 20 MeV with an uncertainty of 30–40 % [7–9]. Also level densities have been derived from fluctuation analysis of total neutron cross sections for a number of nuclei in the same mass range for relatively large ranges of excitation energies with similar uncertainties [10–13].

An alternative method for studying level densities above 20 MeV has been used by Bateman *et al.* [14], in which (n,xp) and $(n,x\alpha)$ spectra are measured for incident energies of 20–50 MeV. The resultant spectra are the sum of many emission stages but do provide some information about level densities at high energies.

Ericson has shown that statistical theory allows the prediction not only of average cross sections, but also of variances of cross sections for reactions proceeding through a compound nucleus. These variances, as well as an average level width also deduced from such analysis, can be used to determine the nuclear level density of the compound nucleus [7,8,15–18].

Beyond mass $A=60$ measurements become increasingly difficult, because with increasing level density the cross sections for any individual exit channel become extremely small. Also the level width decreases strongly with increasing mass number, and above mass $A=60$, Γ becomes smaller than the energy resolution of conventional tandem beams.

The investigation of total neutron cross sections above the single-particle resonance region reveals sharp resonances of several keV width associated with compound nucleus formation, modulated by giant resonances of several MeV width associated with potential scattering as explained by the optical model of the nucleus. In Fig. 1 are shown the fluctuations in the total neutron cross section of natural *S*, as measured in the present experiment. In the region of nonoverlapping levels $(\Gamma<D)$ the reaction proceeds through one particular compound state independent of the others. Agodi and Pappalardo [19] used a method further developed by Carlson and Barschall [10] to analyze the fluctuating cross section in terms of statistical fluctuations in the widths and spacings of the compound nucleus resonances, assuming the energy spacing to be larger than the width of the levels.

In this approach it is assumed that the total cross section can be separated into a slowly varying potential scattering cross section and a rapidly changing compound-nucleus-formation cross section which do not interfere with each other.

With increasing excitation energy the lifetime of the compound system decreases. The energy uncertainty will therefore increase and may be so large that a great number of compound states are contained within it. This is the region of strongly overlapping levels $(\Gamma\gg D)$, the continuum. Consequently it is necessary to consider simultaneous transitions through all states within the region of energy uncertainty and to take interference effects between these states into account. This interference is to a large extent of a random nature and gives rise to fluctuations. The theory of statistical fluctuations has been developed by [16,20–25]. It is assumed that

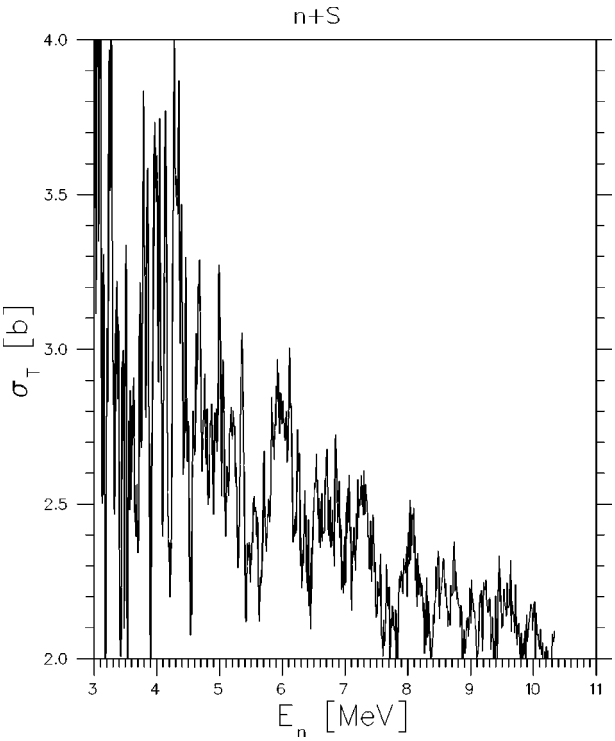

FIG. 1. Fluctuations in the total neutron cross section of natural *S* as measured in this experiment.

the energy resolution is smaller than Γ and, again, that the total cross section can be separated into a direct and a fluctuating part.

In the energy region where the level width Γ is larger than the average spacing *D* between compound nuclear levels, the observed Γ can also be regarded as some average of Γ^J. Consequently, specific reactions used for obtaining excitation functions may not agree with each other in compound nuclear width, if the average compound nucleus spin *J* in the two reactions differs. This width Γ of the compound states is related by statistical theory to a sum of the partial widths of all the exit channels. If the average width Γ of the compound nuclear states is known from cross section fluctuation measurements and information on the exit channels is known from other measurements or theoretical calculations, then the level density of the compound nucleus at a high excitation energy can be obtained.

The average level width Γ can be determined in a number of ways [8,17,18]. The oldest method used for analyzing cross sections is the study of the autocorrelation function. This method is straightforward, but gives rise to large uncertainties in the level width. In the case of very good energy resolution, the ''counting the number of maxima'' method [20,21] provides an alternative for determining the average level width Γ. The most elegant method is Fourier analysis [26] of the excitation function; it not only provides an average level width but also the variance of the cross section free from optical model potential effects.

A comparison of the results of the three techniques indicates consistency between them [27]. All are affected by

poor resolution and/or statistics, but for good data the Fourier series method furnishes smaller errors [18].

It was the goal of this experiment to measure the total neutron cross sections of ^{31}P, ^{32}S, and ^{39}K in the neutron energy range $0.5 \leqslant E_n \leqslant 12$ MeV and the cross sections of ^{51}V, ^{56}Fe, and ^{59}Co in the energy range $0.5 \leqslant E_n \leqslant 3$ MeV. From a fluctuation analysis of pieces of excitation functions, level widths and variances were extracted. The experimental determination of these quantities will allow a judgment on the energy resolution needed for a region, that are suitable for the measurement of nuclear level density data with conventional tandem beams. The experimental determination of level densities then allows comparisons with theoretical predictions, and tests the validity of such predictions about energy and mass dependence of level widths and densities.

Total neutron cross sections were measured at the Ohio University Tandem Accelerator Laboratory. The beam swinger with its 30-m-long time-of-flight tunnel provides an adequate facility to achieve the necessary time-energy resolution.

Experimental level density results will be compared to level densities derived from microscopic calculations based on the formalism of statistical mechanics including a BCS Hamiltonian. Further comparisons will be made with phenomenological models based on the Fermi-gas model.

For the microscopic calculation the code RHOTHERM developed by Grimes and Graham will be used. The code uses the BCS [28] formalism to determine the level density parameter a, the energy shift parameter δ, and the spin cutoff parameter σ.

Numerical calculations starting from the single-particle spectrum given by a shell-model calculation take into account in a natural way the influence of both shell and pairing effects, and also their dependence on the excitation energy. But this approach also has its disadvantages [29], such as the requirement of detailed shell model calculations, resulting in a considerable computational effort, the necessity to adopt normalization procedures in order to be consistent with macroscopic model estimates, and ground state shell and pairing corrections. Also, the statistical mechanical calculation does not take into account collective effects. Therefore, at the present time one cannot fully rely on microscopic calculations.

Alternatively, one can look for simple phenomenological descriptions which take into account the main features of microscopic calculations but remain sufficiently simple for practical applications. A simple model should include the well-known experimental features such as the extremely rapid increase of the level density with energy, odd-even effects, and shell effects. More advanced models should also describe the excitation energy dependence of shell and pairing effects, and the enhancement of the level density because of collective rotations and vibrations.

The statistical properties of excited nuclei are to a large extent similar to those of a degenerate ideal Fermi gas. Simple analytical relations for the state density $\rho_s(E_x)$, the level density $\rho(E_x,J)$, and the observed level density $\omega(E_x)$ for a nucleus with a given excitation energy E_x and angular momentum J can be obtained [30–32].

II. EXPERIMENTAL DESCRIPTION

A. Total neutron cross sections

Total neutron cross sections were determined by measuring the attenuation in the neutron beam by a known amount of material. If N_0 is the number of counts without a sample and N_I is the number with a sample interposed between source and detector, then

$$\sigma_T = \frac{1}{nl} \ln \frac{N_0}{N_I}. \tag{2.1}$$

σ_T denotes the total neutron cross section, n is the number of atoms per unit volume, and l is the length of the sample.

B. Sample characteristics

Samples were chosen according to the following criteria. They are as monoisotopic as possible, easily available, their total neutron cross sections have not been subjected to fluctuation analysis using the techniques described, and theoretical calculations of the level width Γ showed there to be sufficient energy resolution in order to resolve fluctuations ($\Delta E < \Gamma$). The number of samples was determined by the time allotted to this measurement in order to achieve reasonable statistics. Whenever possible, sample lengths were chosen to optimize the total counting time [33]. Sample characteristics are summarized in Table I. The samples were mounted on a 24 in. diameter, four-position aluminum sample wheel, operated by an eight-position Geneva drive. Samples and the open beam-can positions were cycled every 20 sec in order to minimize the effects of beam profile fluctuations. In Fig. 2 is shown the location of the sample wheel with respect to the rest of the experimental setup.

C. Geometry and in-scattering correction

The geometry of the experiment was such as to minimize background and in-scattering by means of proper shielding and neutron beam collimation. Following the neutron beam in Fig. 2 the sample wheel is shielded by two feet of paraffin wax. As in any ''good geometry'' experiment the neutron detector is completely shadowed by the sample, and in the sample out position six feet of polyethylene collimation restricted the neutron flux to less than the diameter of the detector. The collimators, embedded in six feet of reinforced concrete, shielding the time-of-flight tunnel from the neutron source, are conical in shape, starting with 0.5 in. diameter and tapering to 1.07 in. The taper reduces the probability of neutrons being scattered back into the detector solid angle.

For the present geometry the in-scattering contribution was found to be less than 0.1% of the total cross section of natural lead and was therefore neglected.

D. Neutron production

Utilization of a white neutron source in combination with the time-of-flight technique allows for a simultaneous measurement of all neutron energies, binned in 0.48-ns-wide time-of-flight channels, in the energy region of interest. The

TABLE I. Sample characteristics.

Sample	Atomic weight	Isotopic abundance (%)	State	m (g)	Diameter (cm)	$1/nl$ (b/mol)
^{12}C	12.011	98.90	Solid	39.67	2.540	2.548
^{12}C	12.011	98.90	Solid	79.50	2.542	1.273
C_2F_4	100.02	100 for ^{19}F	Solid	61.36	2.548	13.802
C_2F_4	100.02	100 for ^{19}F	Solid	114.95	2.539	7.315
^{31}P	30.974	100	Powder	90.50	2.251	2.262
^{32}S	32.07	95.02	Powder	86.13	2.255	2.469
KF	58.100	93.26 for ^{39}K	Powder	62.81	2.254	6.129
^{51}V	50.942	99.75	Solid	40.15	2.033	6.840
^{56}Fe	55.847	91.72	Solid	182.3	2.539	2.576
^{59}Co	58.933	100	Solid	161.78	2.543	3.072

white neutron source is realized by bombarding a natural Be target (1 in. diameter, 0.08 in. thick) by a pulsed source of protons and deuterons with a burst width of less than 1 ns. A detailed description of the accelerator is presented by Bainum [34].

In both the $^9Be(d,n)^{10}B$ and $^9Be(p,n)^9B$ source reactions, thresholds for several three-body breakup reactions lie below 10 MeV. Thus these reactions produce a considerable number of low energy neutrons [35].

In Fig. 3 is shown the open beam spectrum of the $^9Be(d,n)^{10}B$ (Q value$=4.36$ MeV) and $^9Be(p,n)^9B$ (Q value$=-1.9$ MeV) reaction as detected by an NE213 neutron detector, 1 in. thick, biased at 2 and 0.5 MeV, respectively. The $^7Li(d,n)^8Be$ reaction would have a higher yield and higher energy range [the Q value for $Li(d,n)=15.0$ MeV], but natural Li has a much lower melting point than natural Be (453.7 K as opposed to 1560 K), causing cooling and contamination problems in the projectile beam system.

Unfortunately, because of stability problems with the terminal voltage on the tandem, the maximum deuteron energy was restricted to 7 MeV, resulting in a maximum neutron energy of 11.4 MeV. The $^9Be(p,n)^9B$ reaction was chosen for its negative Q value and high yield in the low-energy region of interest, providing an overlap to the $^9Be(d,n)^{10}B$ reaction at 2 MeV. The proton energy was chosen to be 4.92

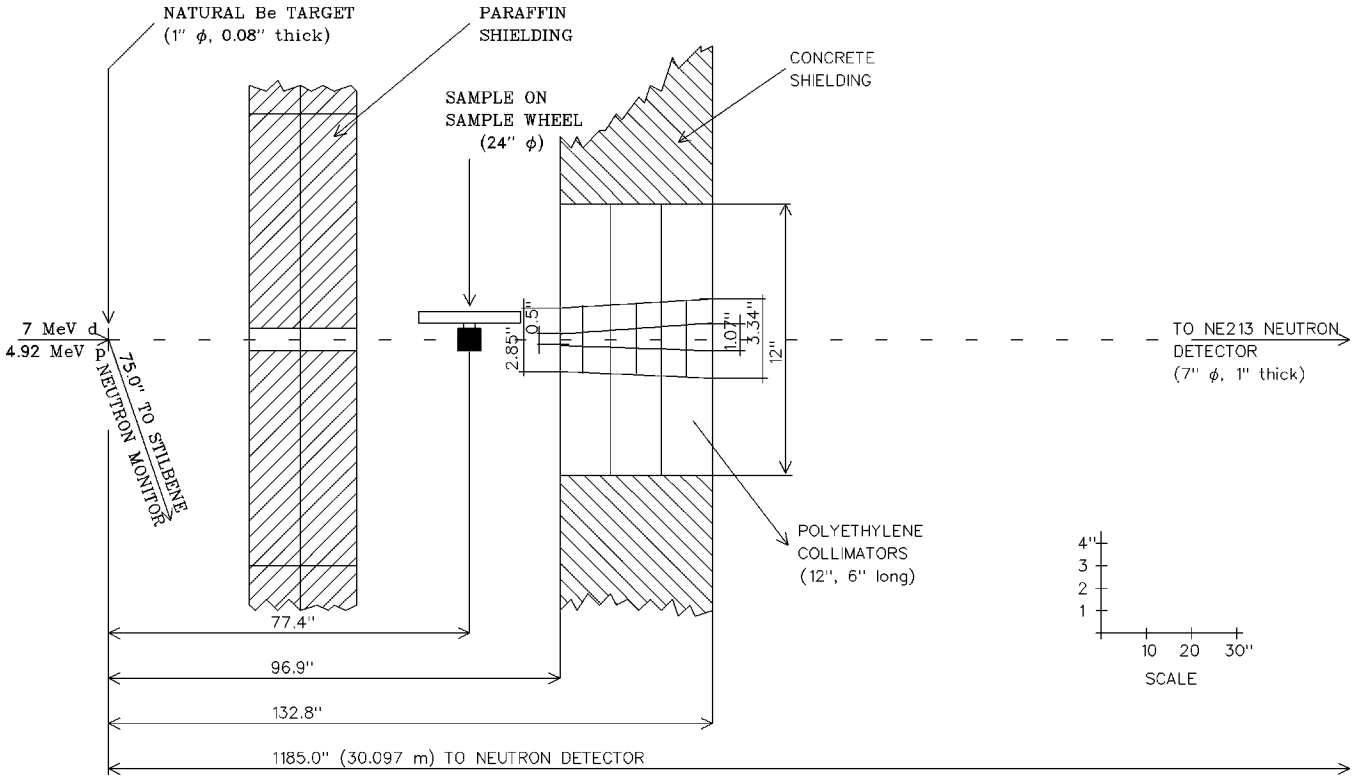

FIG. 2. The experimental setup of the present experiment.

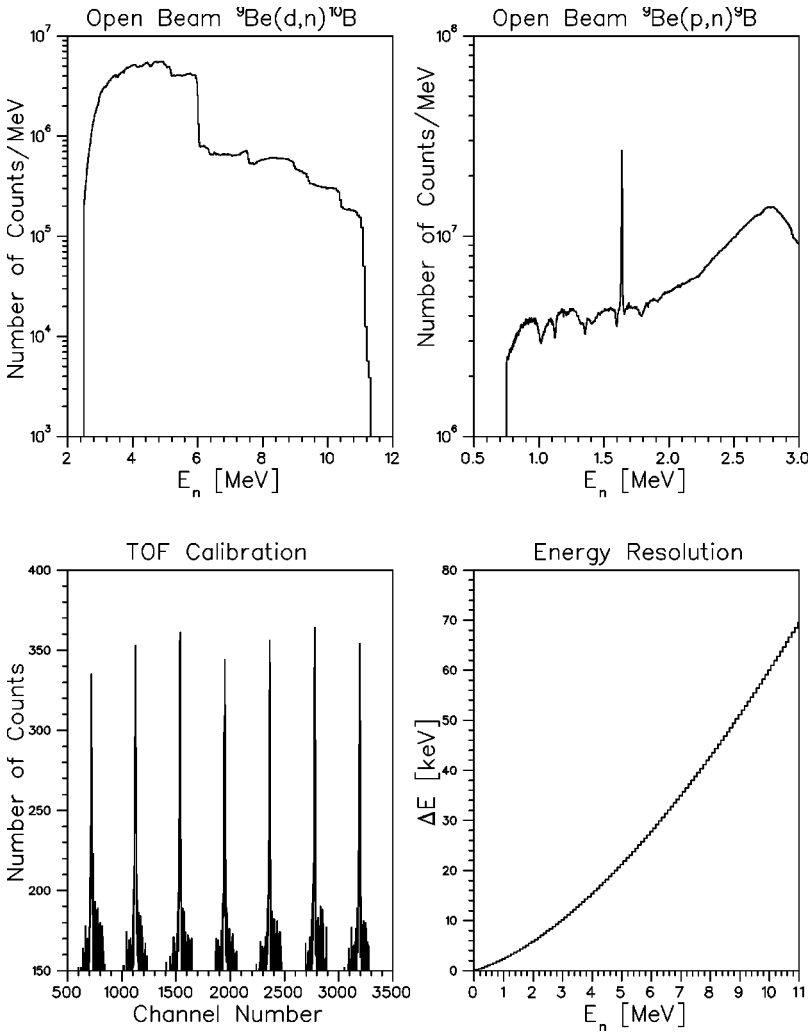

FIG. 3. Top: the open beam spectrum for ^{9}Be$(d,n)^{10}$B and ^{9}Be$(p,n)^{9}$B, as accumulated over 27 h and 39 h, respectively. The sharp peak in the ^{9}Be$(p,n)^{9}$B spectrum is the gamma peak originating from an earlier beam burst. Bottom: the gamma peaks produced by bunching the beam at 5 MHz and stopping the TOF time-to-amplitude converter (TAC) at a rate of 625 kHz, and the energy resolution of the present experiment as a function of neutron energy.

MeV. The range of neutron energies covered is 0.5–11.4 MeV, but statistics are adequate for this analysis only above 0.75 MeV. The average deuteron and proton beam currents were, 330 nA and 400 nA, respectively, at a pulse repetition rate of 625 kHz.

E. Neutron detection and neutron energy

Neutrons were detected using a NE213 liquid scintillator, 1 in. thick and 8 in. in diameter. The scintillator is coupled to a RCA 4522 photomultiplier tube (PMT) with a special bias resistor chain to optimize timing. NE213 has the property of allowing pulse-shape discrimination to separate gammas from neutrons, and also provides excellent timing resolution. The full width at half maximum (FWHM) of the gamma peak was 1.7 ns. In Fig. 3 is shown the energy resolution of the present experiment as a function of neutron energy. Neutron energies were deduced from the time of flight over the flight path. For a description of the time-of-flight technique see [13].

The flight paths in this experiment were $30.097 \pm 0.010/29.996 \pm 0.019$ m, where the solidus notation to the ^{9}Be$(d,n)^{10}$B/^{9}Be$(p,n)^{9}$B setups. Repositioning of the neutron detector was necessary for this work because of other experiments in the time between runs.

F. Electronics and data acquisition

Neutrons are detected via the (n,p) process in the scintillating material NE213 which consists basically of ^{12}C and ^{1}H. The charged particles in return are stopped because of the Coulomb interaction with the scintillator atoms. Consequently the detector is very sensitive to gamma rays, and hence it is crucial to discriminate between gammas and neutrons. Fortunately in NE213, the light decay time for charged particles and gammas is significantly different, allowing for pulse shape discrimination (PSD), and thereby significantly reducing the background.

The electronics (Fig. 4) is designed to provide an interface to the data acquisition system for four sets of signals including, the pulse-shape-discriminated time-of-flight (TOF) signals, the signals associated with the beam monitoring system, the logic handling the sample cycling, and signals to keep track of elapsed time and dead time. For a detailed description of the electronics and data acquisition see [36].

G. TOF calibration

A calibration was obtained by turning off gamma discrimination, directing a beam of 5 MHz repetition rate onto the target and suppressing seven out of eight beam pickoff

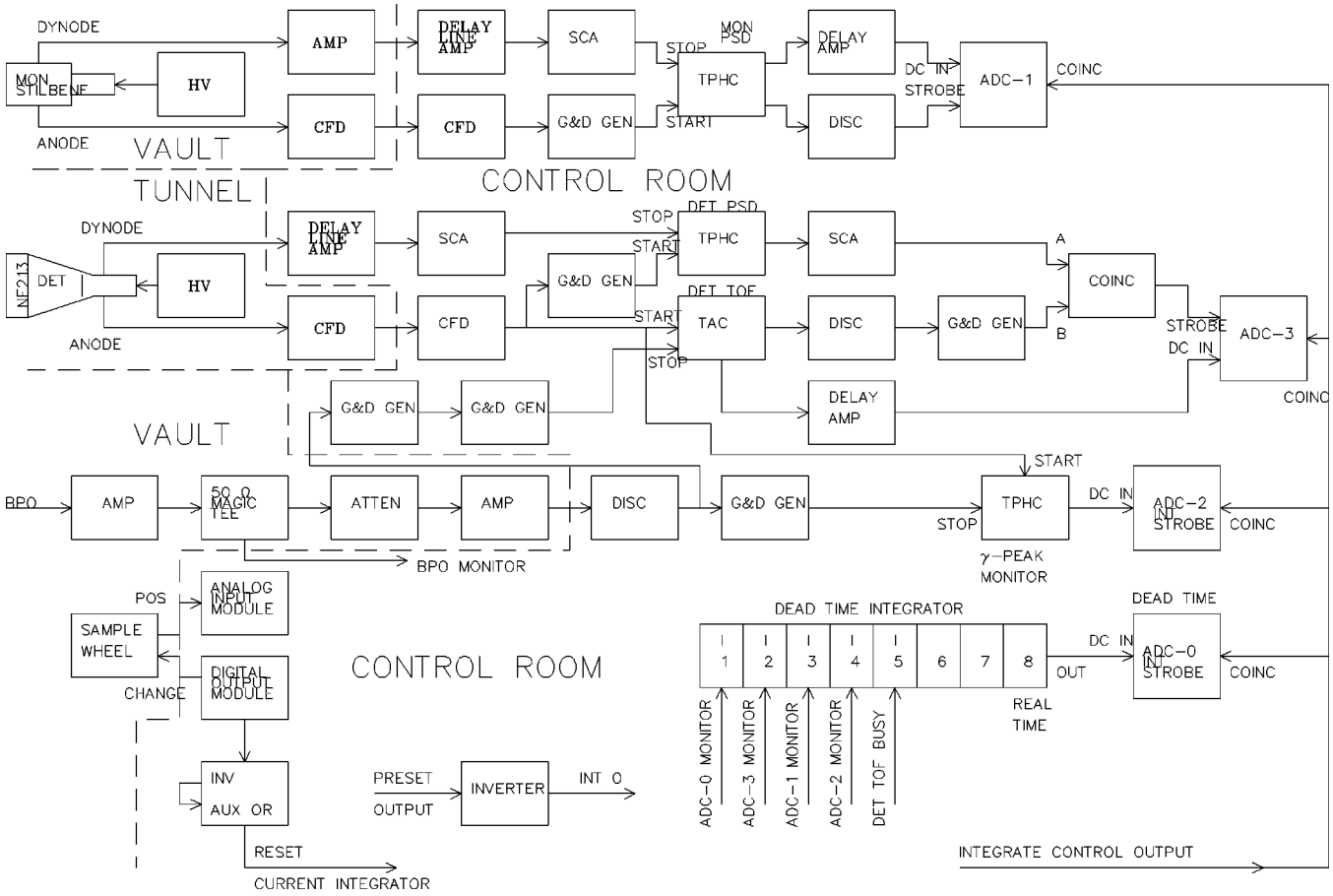

FIG. 4. The electronics diagram for the total neutron cross section measurement.

pulses. This produces peaks at 200 ns intervals across the spectrum. A linear least squares fit yielded a time per channel $\tau = 0.48114 \pm 0.0007$ ns/channel ($\chi^2 = 1.66$) for the ^{9}Be$(d,n)^{10}$B reaction and $\tau = 0.4839 \pm 0.0007$ ns/channel ($\chi^2 = 2.66$) for the ^{9}Be$(p,n)^9$B reaction.

III. THEORY AND DISCUSSION

A. Region of nonoverlapping levels

In the region of nonoverlapping levels ($\Gamma < D$) the reaction proceeds through one particular compound state independent of the others. Agodi and Pappalardo [19] used a method, further developed by Carlson and Barschall [10], to analyze the fluctuating cross section in terms of statistical fluctuations in the widths and spacings of the compound nucleus resonances, assuming the energy spacing to be larger than the width of the levels.

In this approach it is assumed that the total cross section can be separated into a slowly varying potential scattering cross section and a rapidly changing compound nucleus formation cross section which do not interfere with each other. The variance in successive energy bins of the cross section can then be related [37] to the variances in the number and widths of levels, assuming the shape of the level width and level spacing distribution are the same for different quantum numbers; for a given level there is no correlation between partial widths for different quantum numbers, and there is no correlation in the level spacings having the same quantum numbers.

The compound nucleus formation cross section averaged over an energy interval Δ_n, which is much larger than the spacings, and total widths of the compound nucleus levels is given by

$$\sigma_n = \frac{\pi \lambda\!\!\!^{-2}}{\Delta_n} \sum_{J^\pi} g(J) \sum_{ls} \sum_{i=1}^{N^n_{J^\pi}} 2\pi \Gamma_i(ls|J^\pi), \tag{3.1}$$

where

$$g(J) = \frac{2J+1}{2(I+1)}. \tag{3.2}$$

$\lambda\!\!\!^{-}$ is the reduced wavelength, I is the spin of the target nucleus, $N^n_{J^\pi}$ is the number of compound nucleus levels of spin J and parity π in Δ_n, and $\Gamma_i(ls|J^\pi)$ is the partial width for neutron emission into the entrance channel with relative orbital angular momentum l and channel spin s. The subscript i refers to the ith level having spin J and parity π in Δ_n. Although this equation holds strictly only if the levels do not overlap, Bethe [32] has shown that it applies even for overlapping levels if all the partial widths are small compared to their spacings.

A measure of the fluctuations of the cross section is the unnormalized variance F, defined as

$$F=\langle(\sigma_n-\overline{\sigma})^2\rangle, \tag{3.3}$$

where σ_n is the average cross section in the energy interval Δ_n, and $\overline{\sigma}$ is the average compound nucleus formation cross section which is here assumed to be independent of energy. This variance can be related to the variances in the number and width of levels through Eq. (3.1). The result is

$$F=\left[\frac{2\pi^2\lambda\!\!\!^{-2}}{\langle\Delta_n\rangle}\right]^2\sum_{J^\pi} g^2(J)\left\{\sum_{ls}\langle N^n_{J^\pi}\rangle \mathrm{Var}[\Gamma_i(ls|J^\pi)] + [\mathrm{Var}\, N^n_{J^\pi}]\left[\sum_{ls}\langle\Gamma_i(ls|J^\pi)\rangle\right]^2\right\}, \tag{3.4}$$

where $\langle\Delta_n\rangle$ is the average size of the intervals Δ_n, $\lambda\!\!\!^{-}$ is the average reduced wavelength in the interval Δ, which consists of the sum of the intervals Δ_n, and the Γ's are numbered consecutively throughout Δ. The variance (Var) and the average of the neutron widths are taken over the entire interval Δ. With the abbreviations

$$k_w=\frac{\mathrm{Var}[\Gamma_i(ls|J^\pi)]}{\langle\Gamma_i(ls|J^\pi)\rangle^2}, \quad k_n=\frac{\mathrm{Var}\, N^n_{J^\pi}}{\langle N^n_{J^\pi}\rangle}, \tag{3.5}$$

Equation (3.4) may be written as

$$F=(\pi\lambda\!\!\!^{-2})^2\sum_{J^\pi}\frac{g^2(J)}{\langle N^n_{J^\pi}\rangle}\left[k_w\sum_{ls}(T^{J^\pi}_{ls})^2+k_n\left(\sum_{ls}T^{J^\pi}_{ls}\right)^2\right], \tag{3.6}$$

where $T^{J^\pi}_{ls}$ are the transmission coefficients. The transmission coefficients are related to the average spacings of levels D_{J^π} and the average widths by

$$T^{J^\pi}_{ls}=2\pi\frac{\langle\Gamma_i(ls|J^\pi)\rangle}{D_{J^\pi}}. \tag{3.7}$$

For the Porter-Thomas distribution k_w is 2; for the Wigner distribution k_n has the value 0.27. At very high excitation energies where the levels overlap ($\Gamma/D\gg1$), the distributions of both widths and spacings are expected to be exponentials for which both k_w and k_n are unity.

In these equations F is obtained from the experiment; the transmission coefficients are known from optical model calculations, $\langle N^n_{J^\pi}\rangle$, which is essentially the level density is treated as an unknown. In order to evaluate the level density ρ it will be assumed that it is a product of an energy-dependent factor $\omega(E)$ and a spin- and parity-dependent factor $H(J^\pi)$. Gilbert and Cameron's [30] expression for $H(J^\pi)$ was used in the analysis. Then

$$F\Delta_n=\frac{(\pi\lambda\!\!\!^{-2})^2}{\omega(E_n)}\sum_{J^\pi}\frac{g^2(J)}{H(J^\pi)}\left[k_w\sum_{ls}(T^{J^\pi}_{ls})^2+k_n\left(\sum_{ls}T^{J^\pi}_{ls}\right)^2\right], \tag{3.8}$$

with

$$H(J^\pi)=\frac{J+\frac{1}{2}}{2\sigma^2}\exp\left(-\frac{(J+1/2)^2}{2\sigma^2}\right). \tag{3.9}$$

B. Continuum region

As the excitation energy increases, the compound nuclear states broaden and move closer until they finally overlap. The cross section is therefore no longer dominated by a single level but is the product of many nearby levels. This interference is of a mostly random nature and gives rise to the observed fluctuations in the cross sections. The strength of cross section fluctuations depends mainly on the extent to which the nuclear reaction has proceeded through the formation of a compound nucleus. Therefore, the study of fluctuation phenomena provides a way to determine the amount of compound nucleus contribution to the cross section.

At these energies many inelastic channels for compound nuclear decay become available. Consequently, the total width grows and becomes quickly larger than the spacing. In this situation it is no longer possible to separate individual resonances from each other; the cross section is simultaneously dominated by a large number of resonances, the amplitudes of which interfere strongly.

C. Ericson fluctuations

Ericson [16] derived the following expression for the variance of the total cross section:

$$F=\frac{k_w}{\pi\Gamma}\frac{(\pi\lambda\!\!\!^{-2})^2}{\omega(E)}\sum_{J^\pi}\frac{g^2(J)}{H(J^\pi)}\sum_{ls}(T^{J^\pi}_{ls})^2. \tag{3.10}$$

Comparison to the case of nonoverlapping levels shows that Ericson fluctuations produce very similar effects in the total neutron cross section as do fluctuations in neutron widths and level spacings. Investigation of the variance expressions shows the fluctuations to be dampened by the spins of the projectiles and target nuclei. It is thus advantageous to work with zero spin targets and low spin projectiles, everything else being equal. The theory of fluctuations also shows that differential cross sections have larger fluctuations than the integrated cross sections. Also the fluctuations in the integrated cross sections are dampened by the orbital angular momentum channels. The largest fluctuations therefore occur in reactions in which few orbital angular momenta contribute.

D. Γ method

There exists an alternate method for the energy region where the average level width Γ is larger than the average spacing D between compound nuclear levels. The observed Γ can be regarded as some average of Γ^J; i.e., specific reactions used for obtaining excitation functions may not agree with each other in compound nuclear width, if the average J in the two reactions differs. This average width Γ of the compound states is related by statistical theory to a sum of

the partial widths of all the exit channels. Γ^{J^π} and D^{J^π} are related via Blatt [38] and Weisskopf and [16]

$$\Gamma^{J^\pi} = \frac{D^{J^\pi}}{2\pi} \sum_{c''} T_{c''}^{J^\pi}, \tag{3.11}$$

where, according to [39,16], and [40],

$$\sum_{c''} T_{c''}^{J^\pi} \simeq G(J). \tag{3.12}$$

$G(J)$ is given by [39]

$$G(J) = \sum_{b'} \int_0^{U_{b'}^{max}} dU_{b'} \sum_{l_{b'}=0}^{\infty} T_{l_{b'}}^{b'}(\epsilon_{b'}) \times \sum_{S_{b'}=|J-l_{b'}|}^{J+l_{b'}} \sum_{I_{b'}=|S_{b'}-i_{b'}|}^{S_{b'}+i_{b'}} \rho(U_{b'}, I_{b'}). \tag{3.13}$$

b' denotes all the different particles (exit channels) that can possibly be emitted by the compound nucleus. Here J is the angular momentum of the compound states, $I_{b'}$ is the spin of the residual nucleus, $i_{b'}$ is the spin of the ejectile, $l_{b'}$ is the orbital angular momentum in the exit channel, $S_{b'}$ is the channel spin of the exit channel, and $\rho(U_{b'}, I_{b'})$ is the energy- and spin-dependent level density of the residual nucleus formed by emission of particles b' with channel energy $\epsilon_{b'}$. The form and determination of $\rho(U_{b'}, I_{b'})$ will be described in Secs. III F and III G.

Transmission coefficients are calculated using FOP [41], a computer program that solves the three-dimensional Schröedinger equation using the following optical model parameters. For neutrons, the global optical model potential (OMP) parameters provided by Rapaport, Kulkarni, and Finlay [42] are used. Whenever possible, neutron transmission coefficients were derived from specific sets of OMP parameters. For protons, parameters by Perey [43] are used, and for alphas, parameters by McFadden and Satchler [44] are applied.

The transmission coefficient sum $G(J)$ is obtained from a Hauser-Feshbach code HF [45]. HF includes the known level schemes for the lowest 20 levels for the final nuclei reached by the emission of neutrons, protons, alpha particles, and gammas. Levels beyond 20 are included through use of the standard Fermi gas level density expression. $H(J)$ is determined from the spin cutoff parameter in the compound nucleus. The magnitude of the spin cutoff parameter and the level density parameter will be found by calculating the state density using a statistical mechanical code RHOTHERM [45] and then fitting it with the Fermi-gas expression for the state density.

If the average width Γ of the compound nuclear states is known from cross section fluctuation measurements and information on the exit channels is known from other measurements or theoretical calculations, then the level density of the compound nucleus at a high excitation energy can be obtained. A simple averaging procedure is

$$P^J = \frac{(2J+1)T_n^J}{\sum_J (2J+1)T_n^J} \tag{3.14}$$

in

$$\Gamma = \langle \Gamma \rangle = \sum_J P^J \Gamma^J, \tag{3.15}$$

where T_n^J is simply the transmission coefficient for the entrance channel to form the compound nucleus. This averaging procedure has been examined and justified in [13]. Substituting Γ^J with $G(J)D_J/2\pi$ as before, and again assuming that $1/D^J = H(J^\pi)\omega(E)$, leads to

$$\omega(E) = \frac{1}{2\pi\Gamma} \frac{\sum_J (2J+1)T_n^J G(J)/H(J^\pi)}{\sum_J (2J+1)T_n^J}. \tag{3.16}$$

$H(J^\pi)$ is determined from the spin cutoff parameter in the compound nucleus. Thus the observed level density can be determined if transmission coefficients are available. Again, it is implied that the level density of all residual nuclei is known.

Questions regarding the agreement between level densities obtained via the two latter methods have been raised [12,13], and will be further investigated in this work.

E. Determination of the level width (Γ)

The average level width Γ can be determined in a number of ways [8,17,18].

1. Autocorrelation function

The oldest method used for analyzing cross sections is the study of the autocorrelation function

$$F(\epsilon) = \langle [\sigma(E+\epsilon) - \langle \sigma \rangle][\sigma(E) - \langle \sigma \rangle] \rangle = \frac{F(0)}{1 + (\epsilon/\Gamma)^2}, \tag{3.17}$$

where $F(0)$ is the variance of the cross section. By calculating this expression for various values of ϵ, that value for which $F(\epsilon) = F(0)/2$ can be found. This method is straightforward, but not without difficulties. The presence of nonstatistical energy variation of the cross section over energy ranges $\geqslant 10\Gamma$ makes it necessary to choose the averaging interval over which $\langle \sigma \rangle$ is calculated with care.

2. Counting the number of maxima

The method of ''counting the number of maxima'' [20,21] was developed under the assumption of an infinitely good energy resolution and very small statistical errors, so that there are no doubts about the definition of a maximum in

the fluctuating excitation function when counting the number k of peaks per unit energy. Then k is connected with Γ through

$$k=\frac{0.55}{\Gamma}. \tag{3.18}$$

Unfortunately the case of infinitely good energy resolution is an ideal one; it is often difficult to discern a real maximum in the experimental situation where each data point is affected by statistics.

3. Fourier analysis method

A piece of excitation function showing fluctuations can be expressed as a Fourier-transformed time-dependent process [26]. Then expanding the excitation function in the form of a Fourier series,

$$\sigma(E)=\sum_{k=0}^{m} a_k \cos\frac{2\pi kE}{I}+\sum_{k'=1}^{m} b_{k'}\sin\frac{2\pi k'E}{I}, \tag{3.19}$$

where m will be I/d, with I being the energy interval to be expanded, and d being the spacing between points. The Fourier coefficients a_k and $b_{k'}$ are random numbers with a Gaussian distribution, and

$$S_k=a_k^2+b_k^2 \tag{3.20}$$

therefore has an exponential distribution of the form

$$S_k=4\pi\frac{\Gamma}{I}(\mathrm{var}\,\sigma)\exp(-2\pi k\Gamma/I). \tag{3.21}$$

This provides an alternate method for determining Γ.

A comparison of the results of the three techniques indicates consistency between them [27]. All are affected by poor resolution and/or statistics, but for good data the Fourier series method furnishes smaller errors [18]. Statistical errors cause a ''white noise'' contribution in the spectrum, effectively adding a constant to each S_k; therefore a fit is usually made with a constant term added to the right-hand side. Finally, modulation in the energy dependence of the cross section because of optical-model effects or long-range changes in the cross section can affect Γ as well; these can be dealt with by discarding the lowest-order S_k values and fitting only the values beyond a certain S_k, since variations over large energy ranges are seen in low-order k values. Similarly, the variance is also affected by long-range energy modulations. Instead of calculating the variance directly, the value can also be derived from the fit to the $\ln S(k)$ spectrum of the form

$$\ln S(k)=\ln(e^{-Ak+B}+C), \tag{3.22}$$

since once Γ is determined all other quantities are known.

F. Microscopic calculations

Experimental level density results are compared to the level densities derived from microscopic calculations based on the formalism of statistical mechanics including a BCS Hamiltonian. Further comparisons will be made with phenomenological models based on the Fermi-gas model.

For the microscopic calculation the code RHOTHERM developed by Grimes and Graham [45] was used. The code uses the BCS [28] formalism to determine the level density parameter a, the energy shift parameter δ, and the spin cutoff parameter σ. A method developed by Moretto [46] is used to determine the chemical potential of the system, λ, and the gap parameter Δ. Each parameter has a value for protons and one for neutrons. The values of λ and Δ at nuclear temperature $T>0$ are determined by requiring that Δ at $T=0$ be equal to the proton and neutron pairing energies, and using an iterative process to arrive at values for increasing T. The proton and neutron pairing energies of Gilbert and Cameron [30] are usually used. The energies e_k of the single-particle levels are needed in the determination of λ and Δ, and are calculated using the Nilsson model [47] with the single particle levels of Seeger and Perisho [48] or Seeger and Howard [49]. For each λ and Δ (for both protons and neutrons), the energy, the spin cutoff parameter σ, the state density, and the level density are determined.

A realistic treatment of the statistical nuclear properties requires the introduction of residual interactions. The apparently intractable problem associated with many interacting particles in a large spectroscopic space can be overcome by the statistical simplification associated with the central limit theorem. The simplest residual interaction, the pairing interaction, included in the BCS Hamiltonian is of the following form as expressed in the formalism of second quantization:

$$H=\sum_k \epsilon_k(a_k^\dagger a_k+a_{-k}^\dagger a_{-k})-G\sum_{kk'} a_k^\dagger, a_{-k}^\dagger, a_{-k}a_k, \tag{3.23}$$

where ϵ_k are the doubly degenerate single particle energy levels, and $a_{\pm k}^\dagger$ and $a_{\pm k}$ are the creation and annihilation operators. G denotes the so-called pairing strength. Such a Hamiltonian can be approximately diagonalized by means of the quasiparticle transformation described first by Bogoliubov [50]. In such a description, the excitations are considered to be independent fermions whose energy is given by

$$E_k=\sqrt{(\epsilon_k-\lambda)^2+\Delta^2}. \tag{3.24}$$

The logarithm of the grand partition function is then given by

$$\Omega=-\beta\sum_k (\epsilon_k-\lambda-E_k) +2\sum_k \ln[1+\exp(-\beta E_k)]-\beta\frac{\Delta^2}{G}, \tag{3.25}$$

provided that Δ, λ, and β are connected by the following relations:

$$\frac{2}{G}=\sum_{k_N}\frac{\tanh\frac{\beta E_{k_N}}{2}}{E_{k_N}}, \tag{3.26}$$

$$\frac{2}{G}=\sum_{k_Z}\frac{\tanh\frac{\beta E_{k_Z}}{2}}{E_{k_Z}}. \tag{3.27}$$

These equations are usually called the gap equations, since they define Δ, the gap parameter, which is a measure of the pairing correlation. The first integrals of motion and the entropy of the system can be obtained from Ω:

$$N=\sum_{k_N}\left[1-\frac{(\epsilon_{k_N}-\lambda_N)}{E_{k_N}\tanh\frac{\beta E_{k_N}}{2}}\right], \tag{3.28}$$

$$Z=\sum_{k_Z}\left[1-\frac{(\epsilon_{k_Z}-\lambda_Z)}{E_{k_Z}\tanh\frac{\beta E_{k_Z}}{2}}\right]. \tag{3.29}$$

For a particular temperature, this system of equations can be solved simultaneously. β in the above equations is the inverse of the nuclear temperature, N and Z denote the neutron and proton number of the nucleus, and k_N and k_Z represent sums over neutron and proton orbitals. E, the total energy of the system, is derived as

$$E=\sum_{k_N}\epsilon_{k_N}\left[1-\frac{\epsilon_{k_N}-\lambda_N}{E_{k_N}}\tanh\frac{\beta E_{k_N}}{2}\right]-\frac{\Delta_N^2}{G}+\sum_{k_Z}\epsilon_{k_Z}\left[1-\frac{\epsilon_{k_Z}-\lambda_Z}{E_{k_Z}}\tanh\frac{\beta E_{k_Z}}{2}\right]-\frac{\Delta_Z^2}{G}. \tag{3.30}$$

The state density is then

$$\rho_s(E,N,Z)=\frac{1}{(2\pi i)^3}\int d\beta\int d\alpha_N\int d\alpha_Z e^S, \tag{3.31}$$

where

$$S=\beta+\Omega_N+\Omega_Z-\alpha_N N-\alpha_Z Z+\beta E, \tag{3.32}$$

with chemical potentials

$$\lambda=\frac{\alpha}{\beta}. \tag{3.33}$$

Values for G were determined separately for protons and neutrons so as to make Δ at zero energy equal to the pairing energies of Gilbert and Cameron. The saddle point approximation is used to evaluate the integral,

$$\rho_s(E)=\frac{e^S}{(2\pi)^{3/2}D^{1/2}}, \tag{3.34}$$

where D is given by

$$D=\begin{vmatrix}\frac{\partial^2\Omega}{\partial\alpha_N\partial\alpha_N} & \frac{\partial^2\Omega}{\partial\alpha_N\partial\alpha_Z} & \frac{\partial^2\Omega}{\partial\alpha_N\partial\beta}\\ \frac{\partial^2\Omega}{\partial\alpha_N\partial\alpha_Z} & \frac{\partial^2\Omega}{\partial\alpha_Z\partial\alpha_Z} & \frac{\partial^2\Omega}{\partial\alpha_Z\partial\beta}\\ \frac{\partial^2\Omega}{\partial\alpha_N\partial\beta} & \frac{\partial^2\Omega}{\partial\alpha_Z\partial\beta} & \frac{\partial^2\Omega}{\partial\beta\partial\beta}\end{vmatrix}. \tag{3.35}$$

Moretto [46] gives the exact forms of the partial derivatives in the determinant. The spin cutoff parameter can be calculated in the following manner:

$$\sigma^2=\sigma_Z^2+\sigma_N^2, \tag{3.36}$$

with

$$\sigma_N^2=\frac{1}{2}\sum_{k_N}\frac{m_{k_N}^2}{\cosh^2\frac{\beta E_{k_N}}{2}} \tag{3.37}$$

and

$$\sigma_Z^2=\frac{1}{2}\sum_{k_Z}\frac{m_{k_Z}^2}{\cosh^2\frac{\beta E_{k_Z}}{2}}, \tag{3.38}$$

where m_k is the projection of the angular momentum of the kth level. A numerical answer is obtained for the state density, and the nuclear temperature is raised by an appropriate amount to repeat the calculations at the next energy. The level densities obtained from this model are then fit by the Fermi-gas form at high energies and the constant-temperature form at low energies, in order to obtain the parameters a and δ. Finally, the level density $\rho(E,J)$ is related to the state density $\rho_s(E)$ and σ

$$\rho(E,J)=\frac{(2J+1)}{2\sqrt{2\pi}\sigma^3}\rho_s(E)\exp\left[-\frac{(J+1/2)^2}{2\sigma^2}\right], \tag{3.39}$$

following the convention that denotes as a state one of the $2J+1$ degenerate components of a nuclear level of spin J.

As pointed out in the Introduction numerical calculations starting from the single-particle spectrum given by a shell-model calculation take into account in a natural way the influence of both shell and pairing effects, and also their dependence on the excitation energy.

G. Phenomenological models

Simple models should include the well-known experimental features such as the extremely rapid increase of the level density with energy, odd-even effects, and shell effects. More advanced models should also describe the excitation energy dependence of shell and pairing effects, and the enhancement of the level density because of collective rotations and vibrations.

The statistical properties of excited nuclei are to a large extent similar to those of a degenerate ideal Fermi gas. Simple analytical relations for the state density $\rho_s(E_x)$, the level density $\rho(E_x,J)$, and the observed level density $\omega(E_x)$ for a nucleus with a given excitation energy E_x and momentum J can be obtained [30–32]. Gilbert and Cameron give a very detailed derivation for the level density of a gas of neutrons and protons. On the assumption that the single-particle states are equispaced with a density g, one derives, for the level density,

$$\rho(E_x,J)=\frac{(2J+1)}{2\sqrt{2\pi}\sigma^3}\rho_s(E_x)\exp\left[-\frac{J(J+1)}{2\sigma^2}\right], \quad (3.40)$$

with the state density given by

$$\rho_s=\sum_J (2J+1)\rho(E_x,J)=\frac{\sqrt{\pi}}{12}\frac{1}{a^{1/4}E_x^{5/4}}\exp(2\sqrt{aE_x}) \quad (3.41)$$

and finally, for the observable level density,

$$\omega(E_x)=\sum_J \rho(E_x,J)=\frac{\sqrt{\pi}}{12}\frac{1}{a^{1/4}E_x^{5/4}}\exp(2\sqrt{aE_x})\frac{1}{\sqrt{2\pi}\sigma}. \quad (3.42)$$

a is known as the level density parameter and σ as the spin cutoff parameter. Both quantities can be related to the single-particle density g, and σ^2 is the average value of the square of the projections of the angular momentum of the single-particle states lying close to the Fermi energy.

One of the well-known deviations of experimental level densities from the predictions of the Fermi-gas model is that arising from nuclear shell effects. Gilbert and Cameron [30] demonstrated that these deviations are correlated to the ground state pairing and shell correction energies. They based their phenomenological studies on the results from analyzing neutron and proton s-wave resonances in the small energy interval of about 100 keV above the neutron binding energy. Because they only used s-wave resonance data from before 1965, their level density parameters and, with it, their level density predictions are rather unreliable for higher excitation energies. They also assumed the equivalence $\rho^+(E)=\rho^-(E)$, for which there is some contrary evidence as to its validity at 7–8 MeV.

Rohr [51] improves on their results considerably by also correcting for missed levels and including p-wave resonances.

Beckerman [52] also employs level spacing data consisting of s- and p-wave resonances in addition to spacings between levels populated by (d,p) and $(^3\mathrm{He},d)$ reactions transferring one unit of angular momentum, charged particle resonance spacings, and spacings between levels populated by one-nucleon transfer reactions. But his unfortunate choice of parametrization does not allow a meaningful comparison in terms of level density parameters.

Common to all three phenomenological descriptions based on the Fermi-gas model is their lack of an important physical feature: namely, the excitation energy dependence of nuclear shell effects on the thermodynamic properties of the nuclei. Ignatyuk and co-workers [53,54] incorporate this feature by treating the level density parameter a as dependent on both the ground state shell correction energy and the excitation energy of the nucleus. Their model takes also into account the nonlinear dependence of the level density parameter on the mass number A, arising from the finite size of nuclei.

The form for a used is

$$a(E)=a_{eff}\left[1-\frac{\Delta}{E}(1-e^{-\gamma E})\right], \quad (3.43)$$

where $\gamma=0.05$, a_{eff} is the asymptotic value of a at high energies, and Δ is the shell and pairing energy shift. The above form shows an increase of a with E if Δ is positive and a decrease of a with E if Δ is negative. a_{eff} is proportional to A and $A^{2/3}$:

$$a_{eff}=0.0792(A+A^{2/3}). \quad (3.44)$$

IV. DATA AND RESULTS

A. Reduction of data

All data reduction, save the flight path determination, was done using the program WNRVAX.FOR, written for the purpose of total neutron cross section evaluation. Open beam and target spectra were shifted so that their gamma peaks coincide. The time-independent background was subtracted, open beam and target time-of-flight spectra were converted into energy spectra, and the total cross sections evaluated according to Eq. (2.1). The program also includes a full propagation of the statistical error given by

$$\left(\frac{\Delta\sigma_T}{\sigma_T}\right)^2 = \frac{1}{(nl\sigma_T)^2}\frac{1}{(1-d_B/d_O)^2}\left[\frac{1+d_O}{D_O} + \frac{[T+(1-T)d_B/d_O]^2\{1+d_O[T+(1-T)d_B/d_O]\}}{T^2D_x} + \left(\frac{1}{T}-1\right)^2\left(\frac{d_B}{d_O}\right)^2\frac{1+d_B}{D_B}\right], \quad (4.1)$$

where

$$T=\frac{d_x-d_B}{d_O-d_B} \quad (4.2)$$

is the transmission with $d_x=D_x/M_x$ the ratio of detector to monitor counts for measurement with the sample in and $d_O=D_O/M_O$, $d_B=D_B/M_B$ the ratio of detector to monitor counts for open beam and background.

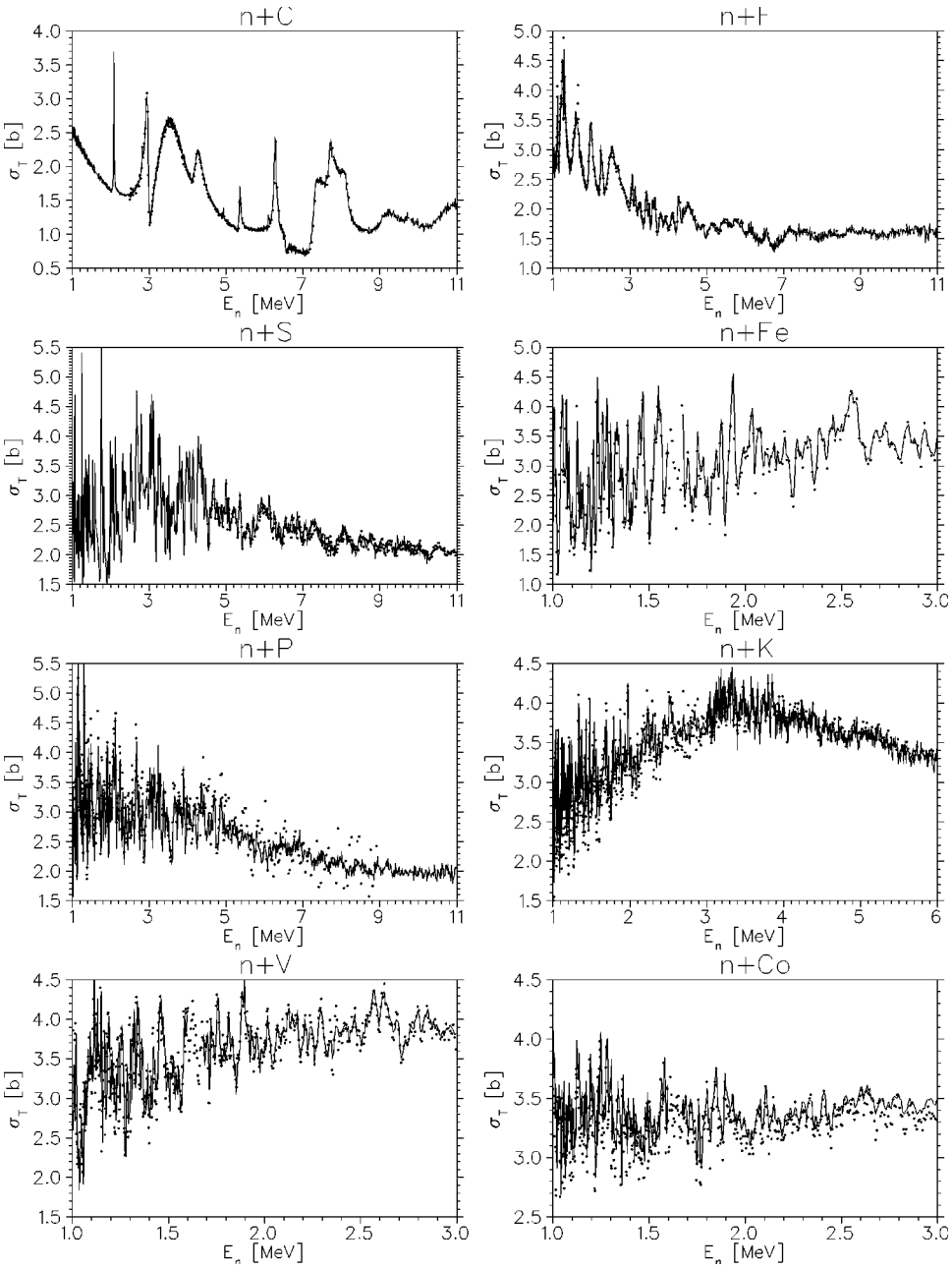

FIG. 5. From top to bottom: present neutron total cross section of natural C and F (solid line), compared to results of Lisowski *et al.* [56] and Larson *et al.* [57] (dotted line), respectively. The total neutron cross section of natural S and natural Fe (solid line). The S cross section is compared with a previous measurement by Carlson and Barschall [10], and the Fe cross section is compared to a measurement by Perey *et al.* [58]. The total neutron cross sections for natural P and K (solid line) compared to measurements by Kellie *et al.* [59] and Kopsch and Cierjacks [11] (dotted line). The total neutron cross sections for natural V and Co (solid line) compared to measurements by Kopsch and Cierjacks [11] (dotted line).

The above expression is easily derived by starting from the expression for the total neutron cross section $\sigma_T = -1/nl \ln T$, and applying standard error propagation techniques.

A note on the background: The ''background'' can generally be regarded as having three components: room background, detector scattered background, and fast background.

The room background consists of neutrons scattered from other experiments, cosmic rays, natural or artificial radioactivities, etc. This background is largely time independent.

The detector-scattered background takes into account the tendency of the detector to scatter a portion of the incident neutrons. These scattered neutrons produce two effects: A neutron resonance will be distorted if the scattered neutrons are detected as they leave the detector system. The scattered neutrons which are moderated by materials outside the detector may then return to be detected at some later flight time. This detector-scattered background is difficult to measure because the insertion of a beam filter or sample removes part of the neutrons which are scattered by the detector. The best approach is proper shielding to minimize the effects of the detector-scattered background. An indication that this produces small effects in the present experiment is the good agreement of sharp structure in the carbon cross section with previous data.

The fast background is essentially caused by neutron leakage from the neutron producing system. This time-dependent background was found to be negligible by using the two-sample technique [55]. Comparison of the cross sections obtained from different sample thicknesses (carbon, teflon) leads to this conclusion.

The total neutron cross sections can be extracted using

two methods in order to verify the hypothesis that rapid cycling minimizes the effects of beam profile fluctuations. Cross sections obtained from the sum of all spectra should be equal to the cross sections derived from a weighted average of all runs analyzed individually. This was verified for the case of natural carbon, whose cross section is very well characterized.

B. Total neutron cross sections: Carbon and fluorine

In Fig. 5 are shown the total neutron cross section of natural carbon. The present data are compared to the results obtained by Lisowski *et al.* [56]. The resonances are very well known, and give therefore a reliable check on the method used to determine the cross sections. All resonances are accounted for and also the magnitude and energy scale is in good agreement with the previous measurement.

A test on the proper extraction of the cross section of an element from a compound is illustrated for the case of fluorine (Fig. 5). The present fluorine cross section is compared to the result obtained by Larson and co-workers [57]. Again the structure and energy scale are in excellent agreement, although there is an overall normalization factor of 0.937 in the Larson data.

The statistical uncertainty for carbon is better than 2% over the entire energy range; for fluorine the uncertainty is better than 2.5%. In general the statistical error is below 2% for all single-element samples (C, P, S, Fe, and Co) and below 3.5% for K (extracted for KF having very low density and C_2F_4). The largest uncertainty was obtained for V, having a thickness well removed from optimum.

C. Total neutron cross sections subjected to fluctuation analysis

In this work the total neutron cross sections of elements in the mass range $32 \leqslant A \leqslant 60$ were subjected to fluctuation analysis. Table II gives a summary of their masses, ground state spin, and parity. Inspection of the ground state spin for the various targets, together with the discussion in Sec. III C on the magnitude of fluctuations as it relates to their dependence on target spin, suggests strong fluctuations in the total neutron cross section of S and Fe. Both targets have zero ground state spin, and investigation of the measured cross sections show indeed very strong fluctuations (Fig. 5).

In the same figure is also shown the total neutron cross section for natural phosphorus compared to the result obtained by Kellie *et al.* [59]. The magnitude and structure are in very good agreement.

Figure 5 also presents the cross section of natural potassium. The observed fluctuations in the cross section of natural potassium are considerably smaller compared to the other targets. The oscillations above 5 MeV are of a purely statistical nature, stemming from the extraction of the cross section from two compounds (C_2F_4 and KF). In the low-energy region there is good structural agreement with [11].

In Fig. 5 is also shown the total neutron cross sections of natural vanadium and cobalt. Comparisons are made with [11]. Structure and magnitudes are again in excellent agreement. Kopsch's data were taken over a flight path of 58 m, resulting in a considerably better energy resolution.

The numerical data files will be deposited in the National Nuclear Data Center at Brookhaven National Laboratory.

D. Determination of the neutron transmission coefficients

Neutron transmission coefficients (ls coupling scheme) were obtained by solving the three-dimensional Schröedinger equation with an optical potential using a conventional parametrization [60]. The optical-model potential is defined as follows:

$$U(r) = V_C - Vf(x_0) + \left(\frac{\hbar}{m_\pi c}\right)^2 V_{SO}(\vec{\sigma}\cdot\vec{l})\frac{1}{r}\frac{d}{dr}f(x_{SO}) - i\left[Wf(x_W) - 4W_D\frac{d}{dx_D}f(x_D)\right], \tag{4.3}$$

where

$$V_C = ZZ'\frac{e^2}{r}\ (r \geqslant R_C) = \frac{ZZ'e^2}{2R_C}\left(3 - \frac{r^2}{R_C^2}\right)\quad (r \leqslant R_C),$$

$$R_C = r_C A^{1/3},$$

$$f(x_i) = (1 + e^{x_i})^{-1} \quad \text{where} \quad x_i = \frac{r - r_i A^{1/3}}{a_i},$$

$$\left(\frac{\hbar}{m_\pi c}\right)^2 = 2.000\ \ (\text{fm})^2. \tag{4.4}$$

The operator σ is defined in terms of the spin angular momentum s as follows.

$s = (\hbar/2)\sigma$ for neutron, protons, ^{3}He, and tritons. $s = \hbar\sigma$ for deuterons, and $s = 0$ for alpha particles.

A is the mass number of the target nucleus.

$V_C(r)$ is the Coulomb potential of a spherical, uniform charge distribution of radius R_C.

The functions $f(x_0)$, $f(x_W)$, $f(x_D)$, and $f(x_{SO})$ are Woods-Saxon form factors with appropriate radius and diffuseness parameters.

TABLE II. Target masses, ground state spin, and parity.

Target		$^{31}_{15}$P	$^{32}_{16}$S	$^{39}_{19}$K	$^{51}_{23}$V	$^{56}_{23}$Fe	$^{59}_{27}$Co
m	[MeV]	28844.44	29773.86	36285.04	47442.63	52090.20	54882.57
I^π		$\frac{1}{2}^+$	0^+	$\frac{3}{2}^+$	$\frac{7}{2}^-$	0^+	$\frac{7}{2}^-$

The imaginary absorptive potential can be either volume ($W \neq 0,\ W_D = 0$), surface ($W = 0,\ W_D \neq 0$), or volume plus surface ($W \neq 0,\ W_D \neq 0$).

Surface absorption can have either a ''derivative-Woods-Saxon'' shape as in Eq. (4.4) or a Gaussian shape.

Reference [36] gives a summary of parameters used in the present calculations. FOP calculates the transmission coefficients in the *ls* coupling scheme. The program FOPTRANS.FOR converted *ls* coupling to *JJ* coupling to be used in Hauser-Feshbach (HF) input files. The effects of the choice of neutron OMP parameters and, with it, neutron transmission coefficients on the final nuclear level density will be investigated in Sec. IV J.

E. Determination of the level widths

The level width Γ and the variance ($\mathrm{var}\,\sigma_T$) of a piece of excitation function encompassing an energy interval I were determined using Eq. (3.22) in Sec. III:

$$\ln S_k = \ln(e^{-Ak+B} + C),$$

where

$$A = \frac{2\pi\Gamma}{I}, \quad B = \ln\left[4\pi\frac{\Gamma}{I}(\mathrm{var}\,\sigma_T)\right] \tag{4.5}$$

or, solving for Γ and $\mathrm{var}\,\sigma_T$,

$$\Gamma = \frac{I}{2\pi}A, \quad \mathrm{var}\,\sigma_T = \frac{I}{4\pi\Gamma}e^B. \tag{4.6}$$

The uncertainty in the level width ($\Delta\Gamma$) is easily calculated by assuming that only the first M' points of the spectrum S_k essentially fix the widths Γ, that is, the slope of the logarithm of the spectrum where M' is defined such that $k \gg M'$ if $\exp(-2\pi k\Gamma/I) < C$. Then

$$\Delta\Gamma = \pm\sqrt{\frac{3I^2}{\pi^2 M'^3}}$$

with

$$M' = \frac{B - \ln C}{A} \simeq \frac{\ln C}{A} = \frac{I}{2\pi\Gamma}\ln C. \tag{4.7}$$

Therefore the $\ln S_k$ spectra should show a clear separation into a straight line and noise segment. In Fig. 6 is shown the $\ln S_k$ spectra for P for several energy intervals with minimum k's successively removed. Inspection of the graphs reveals the expected separation.

To take into account the effects of finite energy resolution on the determination of the level width gamma, a method was developed by Lang [61] for the autocorrelation method. In his study he assumed different resolution functions (box, Lorentzian, and Gaussian). An attempt was made by Grimes [62] to investigate the effects of finite energy resolution on the level widths extracted from the Fourier series method on a theoretical basis. By assuming a Gaussian resolution function with variance σ^2 of the functional form

$$R(\epsilon) = \frac{1}{\sqrt{2\pi}\sigma}\exp\left(-\frac{\epsilon^2}{2\sigma^2}\right), \tag{4.8}$$

he arrived at a resolution factor of the form

$$f(k) = \exp\left[-\left(\frac{2\pi k\sigma}{I}\right)^2\right]. \tag{4.9}$$

This factor represents a reduction in S_k due to the finite resolution. Inclusion of Eq. (4.9) leads to the following modification of Eq. (3.22):

$$\ln S_k = \ln(e^{-Ak-Dk^2+B} + C). \tag{4.10}$$

Fits to the $\ln S_k$ values from the Fourier series expansion were calculated for several minimum k values. Elimination of the first few values improved the χ^2 for the fit of Eq. (3.22) to the data. As the best level width the value was chosen where the χ^2 stabilized and successive k removals did not alter gamma considerably. This value together with the value for $\mathrm{var}\,\sigma_T$ (S_0) was used to deduce the level density.

Note that this value for the variance is different from the one that would be calculated from the cross section data. Deletion of the first few k values in the Fourier analysis of the cross section is equivalent to removing the potential scattering contribution to the cross section, which results in a different variance.

The effects of finite energy resolution were investigated for all the compound nuclei of interest. D was chosen to be a fixed parameter, since it was uniquely determined by the known energy interval and energy resolution. Good convergence of the least squares fits to the $\ln S_k$ spectra was found with a slightly better χ^2 than for the case without incorporation of the energy resolution function. For $A \leqslant 40$ a less than 5% change resulted in the extracted gamma values, whereas for $A \geqslant 40$, changes of up to 40% were observed. Also affected by the introduction of the energy resolution function was the extracted variance, with generally larger values than found without the extra factor, but with considerably lower variation than was observed in the change of gamma values. The white noise contribution remained virtually unaffected.

As a consequence, introduction of the energy resolution factor considerably improved the agreement between the variance and gamma method, as observed in the final level densities, especially for $A \geqslant 40$.

Table III summarizes the extracted gamma values for the present experiment as a function of excitation energy.

F. Variance method

Equation (3.10) gives the variance of the total neutron cross section for overlapping levels ($\Gamma \gg D$). Here F can be related to

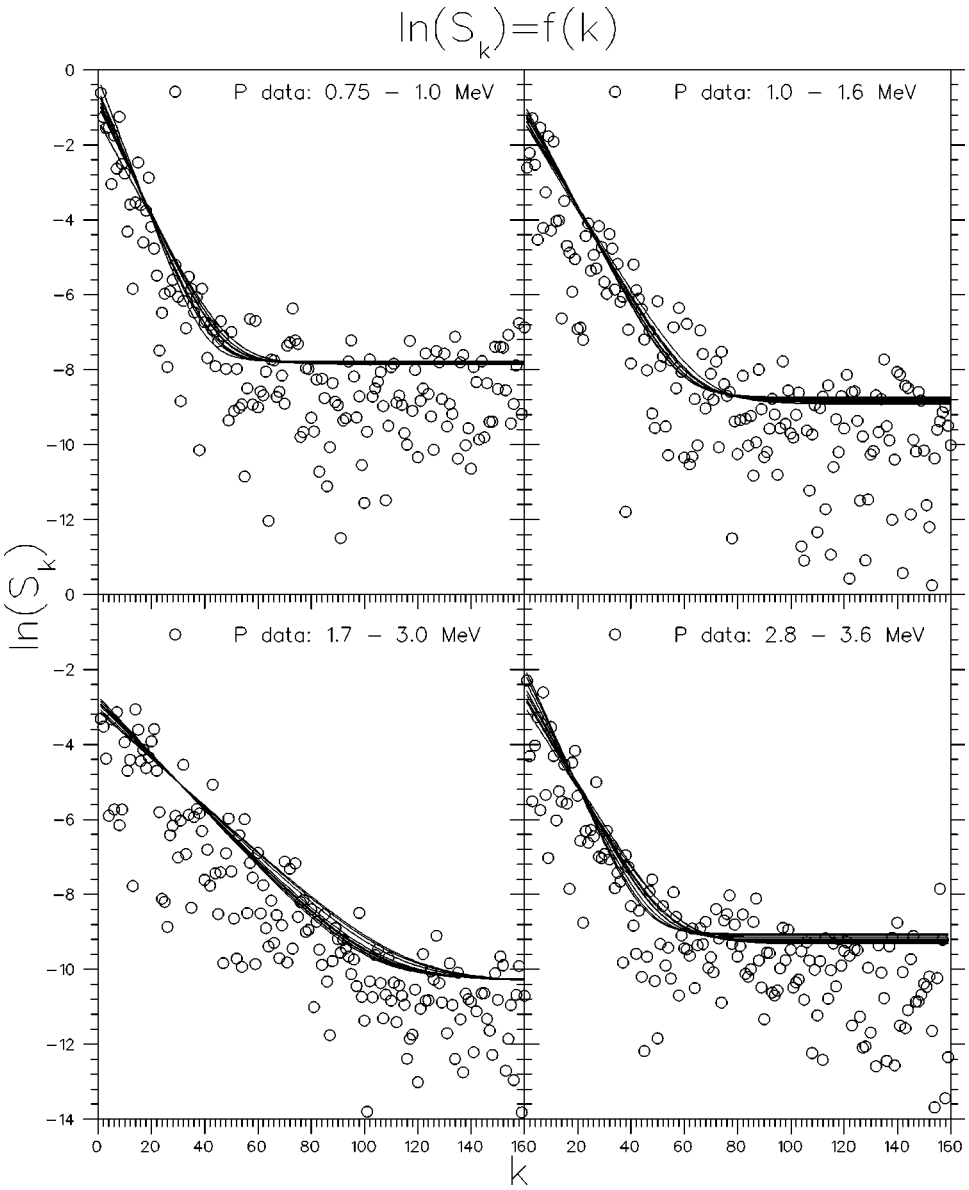

FIG. 6. The $\ln S_k$ plots of P for several energy intervals I ($0.75 \leqslant E_n \leqslant 3.6$ MeV); the solid lines are the least squares fits to the present data according to Eq. (3.22).

$$S_0 = a_0^2 + b_0^2 = e^B + C = 4\pi \frac{\Gamma}{I} \text{var}\, \sigma_T + C. \qquad (4.11)$$

Then solving for the variance and substituting into Eq. (3.22) leads to the following result for the observable level density:

$$\omega(E) = \frac{4}{(S_0 - C)I} (\pi \lambda\!\!\!^{-2})^2 \sum_{J^\pi} \frac{g^2(J)}{H(J^\pi)} \sum_{ls} (T_{ls}^{J^\pi})^2. \qquad (4.12)$$

A word on the variance: If the target sample consists of several isotopes, then the cross section must be considered separately for each isotope. The variance of the isotopic mixture is easily found by adding the variances for each isotope weighted by the square of the isotopic abundance. In the present work, the samples for which fluctuations were analyzed are either monoisotopic or one isotope was sufficiently abundant so that the contributions to the variance from the remaining isotopes were negligible.

S_0 is known from a fit to the $\ln S_k$ spectra, and the transmission coefficients were obtained from FOP; therefore the only additional parameter needed is the spin cutoff parameter, in order to specify $H(J^\pi)$. The single-particle energies proposed by Seeger and Perisho [48] and Seeger and Howard [49] were used to calculate the spin cutoff parameters using the microscopic Fermi gas code RHOTHERM [see the Introduction and Sec. III F, Eq. (3.36)]. Relatively small uncertainties were found in the spin cutoff parameters ($<8\%$) based on the comparison between the two single-particle sets. The spin cutoff parameter (σ), obtained from the Seeger-Howard single-particle energy sets, was used to calculate the level densities denoted by the variance method. Other uncertainties could come from the fact that the derivation of Eq. (3.10) assumes that the total level width is independent of J, which allows Γ to be factored out of the sum. If this assumption is relaxed, the sum can be evaluated using

TABLE III. The level widths (Γ) of the present experiment.

	^{32}P			^{33}S			^{40}K	
E_x [MeV]	Γ [keV]	$\Delta\Gamma$ [keV]	E_x [MeV]	Γ [keV]	$\Delta\Gamma$ [keV]	E_x [MeV]	Γ [keV]	$\Delta\Gamma$ [keV]
8.815	8.3	0.7	9.52	4.9	0.4	8.68	5.9	1.4
9.226	9.8	0.6	9.94	6.1	0.4	9.10	4.1	0.6
10.20	13.1	0.6	10.91	21.1	1.2	10.08	13.5	1.7
11.04	13.6	1.2	11.75	9.9	0.7	10.29	8.0	2.5
12.05	21.8	1.6	12.76	25.5	1.5	11.94	11.4	2.2
13.70	21.8	2.3	14.41	25.7	2.0			
16.64	73.9	14.3	17.36	58.2	12.9			
	^{52}V			^{57}Fe			^{60}Co	
E_x [MeV]	Γ [keV]	$\Delta\Gamma$ [keV]	E_x [MeV]	Γ [keV]	$\Delta\Gamma$ [keV]	E_x [MeV]	Γ [keV]	$\Delta\Gamma$ [keV]
8.20	3.7	0.4	8.54	2.7	0.3	8.38	2.3	0.2
8.62	3.3	0.4	8.96	4.5	0.2	8.80	3.7	0.4
9.60	11.7	1.2	9.94	10.5	0.5	9.78	9.3	1.0

the relative J dependence predicted by a Hauser-Feshbach calculation. In the present study it was found that with increasing excitation energy less than 15% changes resulted from this alternative calculation.

G. Gamma method

Evaluation of the level densities from the gamma values is carried out following the approach outlined in Sec. III D. Level density information on the exit channels $\rho(U_{b'})$ is again obtained from RHOTHERM. The binding energies were obtained from Nuclear Data Tables [63] and gamma decay chains form the Table of Isotopes [64].

In the past it has been common to average lifetimes rather than widths [65], in which case

$$\frac{1}{\Gamma} = \sum_J \frac{P_J}{\Gamma_J}. \tag{4.13}$$

If one constructs an autocorrelation function from equal contributions of functions with two or three different widths, the best fit gamma is actually between the two approaches, although the difference between the two gamma values is normally less than 25%, making the distinction less important. As pointed out in Sec. III, the validity of the present approach was verified in [13]. The agreement between the two averaging procedures, again, improves with increasing excitation energy. Level densities were calculated using both values and the average was denoted as the level density obtained from the gamma method.

A far more important question is that of level densities in the residual nucleus. As can be seen from the formula for $\omega(E)$, the level density varies linearly with the sum of the transmission coefficients over all outgoing channels. For the lowest energies, the Hauser-Feshbach calculation depends only on known levels, while as the energy increases, the largest decay branches move to regions in the continuum. The present calculations include the lowest 20 levels in each final nucleus as individual levels, with the continuum formula used beyond this point.

H. Results: Comparison to phenomenological and microscopic calculations

Calculations were carried out with the tabulation of Rohr [51], Gilbert and Cameron [30], Beckerman [52], Ignatyuk *et al.* [54], and with parameters obtained from statistical mechanical calculations with the single-particle states proposed by Seeger and Perisho [48] and Seeger and Howard [49]. In general, the various predictions show a consistent shape, but differ in magnitude.

The general trend of the values obtained from the fluctuation analysis follows the slope predicted by statistical mechanical calculations and by compilations. In general there is good agreement (except for potassium) between the Seeger-Howard (SH-SPL) and Seeger-Perisho (SP-SPL) tabulations. With increasing mass number considerable improvement in the agreement between phenomenological tabulations and the microscopic calculations becomes noticeable, in particular this is true for the compound nuclei ^{52}V, ^{57}Fe, and ^{60}Co.

The values deduced from the gamma technique are almost completely insensitive to the choice of level density parameters in the residual nuclei at the lower energies (where only the tabulated level energies are used); only at the highest energy is there an indication of divergence, as can be seen in the case of ^{32}P and ^{33}S. This is as expected, since the level density values in the compound nucleus of a given value of gamma show a linear dependence on the level densities in the residual nuclei. Consequently, in this energy range, the level density results depend sensitively on the assumed final nucleus level densities with the gamma method. A great advantage of the variance method is that the residual level densities do not enter into the calculation. Therefore, at the highest energies, the uncertainty in the values of the level density deduced from the gamma method increases substantially, while that for values obtained from the variance method should remain roughly the same until the fluctuations become too small to measure reliably.

There is good agreement between the two techniques for ^{32}P and ^{33}S, as well as good agreement with the compilations by Rohr and Gilbert and Cameron. With increasing A there is a noticeable divergence between the two methods with level densities derived from the variance method being consistently higher, but still in good agreement with the values derived by Ignatyuk *et al.* [54].

Figure 7 gives an overview as to how the present level density results compare to one another, and to microscopic and phenomenological calculations. To check on the validity of the assumption of overlapping levels ($\Gamma > D$), the values Γ/D_J were calculated for ^{32}P and ^{60}Co for $0 \leqslant J \leqslant 7$. It was

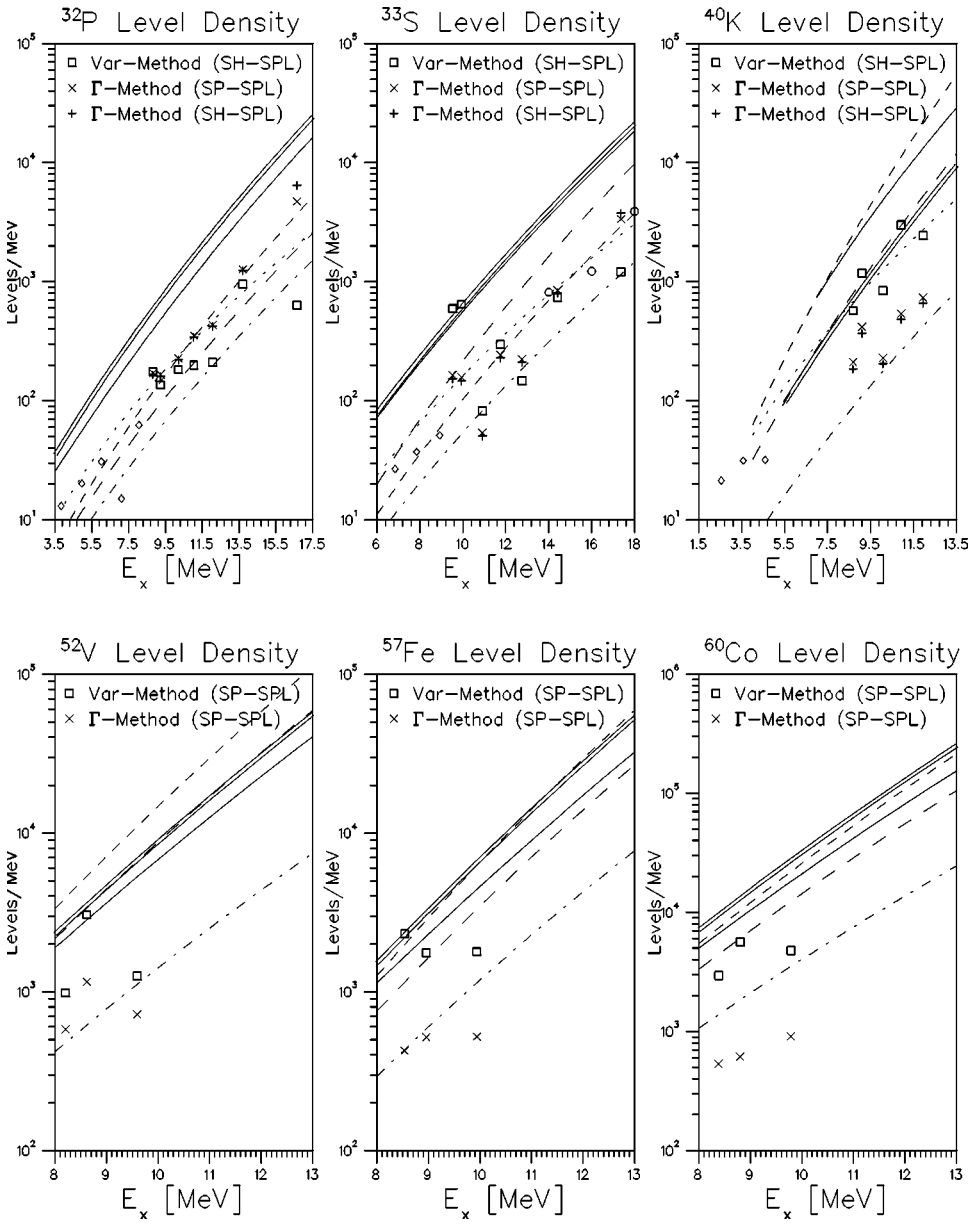

FIG. 7. The present nuclear level densities of ^{32}P, ^{33}S, ^{40}K, ^{52}V, ^{57}Fe, and ^{60}Co, compared to microscopic and phenomenological calculations. Solid and double-solid lines denote the microscopic calculations with Seeger-Perisho [48] and Seeger-Howard [49] levels, respectively. The long-dashed, short-dashed, dot-dashed, and dotted curves show the predictions of Gilbert and Cameron [30], Rohr [51], Ignatyuk *et al.* [54], and Beckerman [52], respectively. The □ symbols denote values obtained from the variance method. The × and + marks denote values derived from the gamma method with level densities in the final nuclei given by microscopic predictions based on Seeger-Perisho [48] and Seeger-Howard [49] single-particle states, respectively. Also shown is a comparison to the tabulated low-energy data by Endt (◇) [66] and level densities obtained by Carlson and Barschall (○) [10].

found that $\Gamma/D_J > 1$ for virtually all excitation energies and J values.

I. Comparison to tabulated levels

A broader test for the level density predictions can be made with the use of low-energy level density data gathered by Endt [66]. The levels listed were summed to obtain values for the level density in the region below 8 MeV excitation energy for ^{32}P, ^{33}S, and ^{40}K. In the case of $A > 40$ nuclei, large numbers of missing levels made a meaningful comparison to low-energy level density data impossible.

The results are again shown in Fig. 7. Inspection of the graphs indicates consistency with the higher-excitation-energy data and compilations.

The unorthodox level density form used by Beckerman may explain why the level density for his parameters has a somewhat different shape. A comparison is also made with the results of Ignatyuk and co-workers [54]. These authors propose that an energy-dependent a be used to deal with shell and collective effects. The form for a used is given by Eq. (3.43) with a_{eff} given by Eq. (3.44). The agreement with this parametrization becomes better with increasing A.

J. Influence of the choice of OMP parameters on the nuclear level densities

FOP allows the reconstruction of the total neutron cross section from the neutron transmission coefficients obtained from a set of OMP parameters. The cross sections so obtained were compared to the measured total neutron cross sections. Generally, agreement between measured and calculated cross section was found to be better than 10%. Also, agreement between cross sections obtained from different parameter sets was of the same magnitude. As a further check, the influence of the imaginary part of the optical

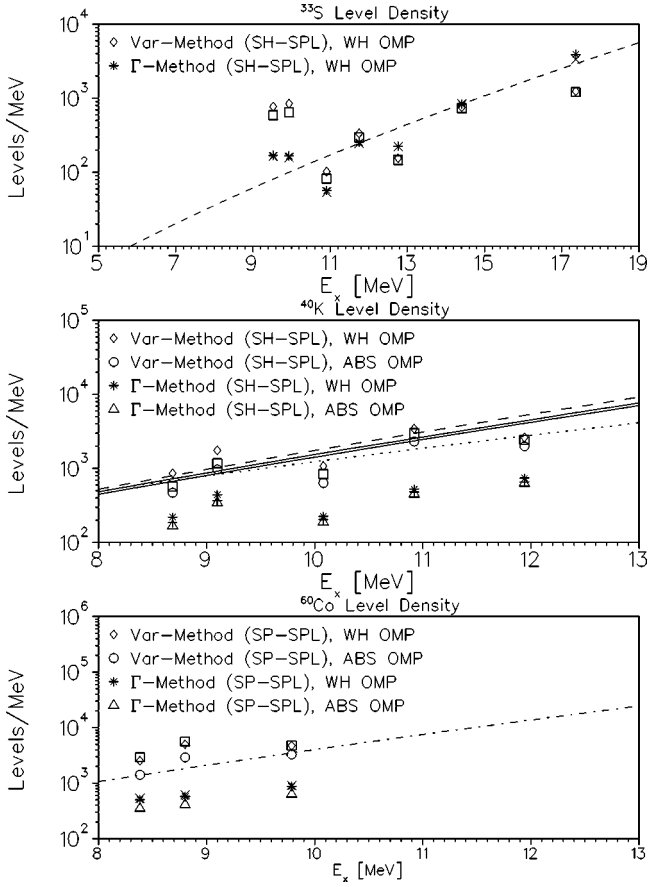

FIG. 8. Shown are the data points presented in Fig. 7 which are based on the Rapaport-Kulkarni-Finlay [42] OMP parameter set. The ◇ and * symbols denote results from the variance method and gamma method, respectively, both based on the Wilmore-Hodgson (WH) [67] OMP parameter set. The single-particle states used in the calculations are from Seeger and Howard [49] for ^{33}S and ^{40}K, and from Seeger and Perisho [48] for ^{60}Co. The ○ and △ symbols denote results from the variance method and gamma method, respectively, both based on the ABS [68] OMP parameter set. The single-particle states used in the calculations are from Seeger and Howard [49] for ^{40}K and from Seeger and Perisho [48] for ^{60}Co.

model potential on the total neutron cross section was investigated and showed the cross sections fairly insensitive to the choice of the imaginary strength.

In order to investigate the effects of the choice of neutron OMP parameters on the final nuclear level densities, several parameter sets were used besides the one by Rapaport, Kulkarni, and Finlay [42]. Figure 8 compares level densities derived from Wilmore and Hodgson [67] to the above-mentioned parameter set. As can be seen from [36], the difference in the real strength is approximately 10%, whereas the difference in the surface strength is more than 50%. Inspection of Fig. 8 shows a difference in the level densities of 20% for the variance method and less than 5% for the gamma method at the low-energy end. With increasing excitation energy, virtually no differences are discernible.

The large uncertainty in the variance method is not surprising, since the level density obtained from this method depends quadratically on the transmission coefficients, whereas the dependence in the gamma method is only linear. Also, at the low-energy end a slight improvement in the agreement between the two methods is noticeable.

The effects of local OMP parameter sets were investigated for ^{40}K and ^{60}Co. Neutron transmission coefficients were obtained from a parametrization by Smith of ^{45}Sc and ^{58}Ni [68,69]. Again there are large differences in the strength of the imaginary term for the various sets (see Ref. [36] for details). Inspection of Fig. 8 reveals the gamma method to be far less sensitive to the choice of OMP parameters, whereas for the variance method far more divergence in the level density values obtained from the three parametrizations is observable. The agreement between the two methods improves with excitation energy and choice of a local (one particular A) OMP parameter set, instead of global OMP parameter sets. In summary, care must be taken in the choice of OMP parameter sets.

K. Extraction of level density parameters for ^{32}P, ^{33}S, and ^{40}K

Finally level density parameters (a, a_{eff}, and Δ) were extracted for ^{32}P, ^{33}S, and ^{40}K. (Fig. 9). The fit marked ''Rohr fit'' uses the conventional (constant a) Fermi gas form, since the starting points for the parameters a and Δ were the values of Rohr [51]. The fit marked ''Ignatyuk fit'' finds the least squares to the present data by varying a_{eff} and again Δ.

The fitting procedure applied is the same as used for the $\ln S_k$ least squares fits, namely, the Gauss-Newton method [70]. The fits produced similar quality representations of the data and are consistent roughly with $a=A/9$ and backshifted values for Δ (i.e., more negative than the usual 0 for odd-odd, Δ for even-odd or odd-even, and 2Δ for even-even nuclei). Table IV summarizes the extracted level density parameters of ^{32}P, ^{33}S, and ^{40}K.

V. SUMMARY AND CONCLUSIONS

The total neutron cross sections of ^{31}P, ^{32}S, ^{39}K, ^{51}V, ^{56}Fe, and ^{59}Co have been measured in the neutron energy range $0.75 \leqslant E_n \leqslant 11.3$ MeV using a white neutron source and standard time-of-flight techniques. The white neutron source was created utilizing the ^{9}Be$(d,n)^{10}$B and ^{9}Be$(p,n)^{9}$B reactions.

The resulting total neutron cross sections were subjected to fluctuation analysis in order to extract level width and level density information for the compound nuclei ^{32}P, ^{33}S, ^{40}K, ^{52}V, ^{57}Fe, and ^{60}Co in the excitation energy range $8.5 \leqslant E_x \leqslant 18$ MeV. Fourier analysis of excitation function energy intervals allowed the extraction of average level widths (Γ) and cross section variances.

Nuclear level densities were obtained on the assumption of overlapping levels via their relationship to the variance of the total neutron cross section (variance method) as predicted by the fluctuation theory of the compound nucleus. Also level densities were obtained via their relationship to the average level widths (gamma method) as predicted by compound nuclear theory.

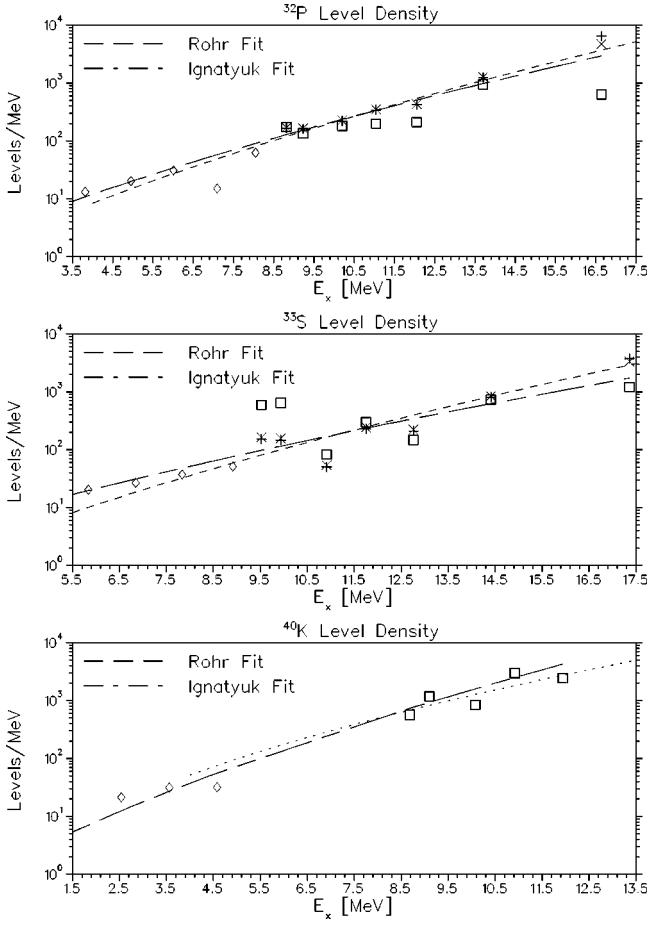

FIG. 9. From top to bottom: least squares fits to the present level density data of ^{32}P, ^{33}S, and ^{40}K. Shown are the data points presented in Fig. 7 and the predictions of Rohr [51] (dashed line) and Beckerman [52] (dotted line), and a fit optimizing the representation of the data by varying a and the energy shift Δ (long-dashed line). The dot-dashed line shows a fit based on the formalism of Ignatyuk, Smirenkin, and Tishin [53] where both a_{eff} and Δ are varied.

The present study shows good agreement between the gamma and variance method for ^{32}P and ^{33}S. As the mass number increases there is a noticeable divergence between the two methods, with the variance method giving consistently higher results.

Limitations notwithstanding, the present data do extend the knowledge of nuclear level density data into a previously unexplored region and allow an evaluation of the many published microscopic and phenomenological estimates. Among the phenomenological tabulations, the parametrization of Beckerman is the most reliable when it comes to reproducing the present level density data for $A \leqslant 40$. The Rohr parametrization is in good agreement with the level density data of ^{32}P and ^{33}S, but overestimates the ^{40}K data by as much as a factor of 5. The values derived from the Gilbert-Cameron parametrization appear to be the least reliable in reproducing the present data. Above $A > 40$ evaluation of a particular phenomenology becomes difficult because of the large dispersion in the present data, but in contrast to $A \leqslant 40$ level density data, the parametrization of Ignatyuk *et al.* provides the closest representation of the present results.

As can also be seen from this study, microscopic calculations based on the single-particle energy sets of Seeger and Howard and Seeger and Perisho are rather density predictions which are too high in the entire mass and energy region of interest, although they provide a fair representation of the derivative of the level density with respect to energy.

It appears that reliable level density data may be obtained over a range of $\simeq 10$ MeV from total cross section measurements for $A \leqslant 40$, but the errors are still approximately 30–40 %. This figure was arrived at by an empirical estimate along the lines as presented by Vonach [71], who assigned uncertainties to the individual components involved in the calculation of the final nuclear level densities, namely, OMP parameters, residual level densities in the Hauser-Feshbach sum, spin cutoff parameters, uncertainty in the variance and level width because of statistics, etc. Nonetheless, such measurements reach an energy region which is difficult to study using other techniques and are particularly valuable.

For the heavier nuclei ($A > 40$) in this study, assignment of uncertainties becomes problematic. As has been demonstrated, inclusion of an energy resolution factor in the Fourier method and realistic sets of OMP parameters only partly resolved the discrepancy between the variance method and gamma method, on the one hand, and the experimental values and phenomenological models on the other.

It was found that the variance method is far more sensitive to the choice of OMP parameters than is the gamma method, whereas in the case of the correction for finite energy resolution the opposite was observed to be true.

From this it can be concluded that in order to obtain reliable level density information for nuclei with $A > 40$, from the fluctuation analysis of total neutron cross sections, improvements in the energy resolution and statistics are para-

TABLE IV. Level density parameters of ^{32}P, ^{33}S, and ^{40}K.

	^{32}P		^{33}S		^{40}K	
	a or a_{eff} [1/MeV]	Δ [MeV]	a or a_{eff} [1/Mev]	Δ [MeV]	a or a_{eff} [1/MeV]	Δ MeV
Seeger-Perisho	4.24	-1.35	5.49	2.38	7.71	2.76
Seeger-Howard	4.44	-1.50	5.14	1.47	6.30	1.95
Rohr	3.92	0.0	3.98	1.62	6.58	1.64
Rohr fit	3.58 ± 0.22	-1.20 ± 0.70	3.21 ± 0.23	-1.24 ± 0.91	5.08 ± 0.32	-0.82 ± 0.60
Ignatyuk fit	3.47 ± 0.30	-1.04 ± 0.62	3.12 ± 0.29	-1.06 ± 0.76	4.93 ± 0.40	-0.77 ± 0.52

mount. This is necessary in order to compensate for the greatly reduced widths and smaller fluctuations in the cross sections. Alternatively, with similar time resolution, the neutron energy range of interest could be shifted downwards.

Also, the analysis of fluctuation data on partial cross sections through the same compound nuclei would be helpful, since this would not only provide additional level density values, but would also provide constraints on the residual level densities if the average cross sections are matched. Partial cross sections are harder to measure, but the fluctuations are much larger. This statement is particularly true for $A \geqslant 40$.

ACKNOWLEDGMENTS

The authors would like to recognize Don Carter and Dave Sturbois for their tireless efforts in keeping the data acquisition and accelerator running.

[1] W. Hauser and H. Feshbach, Phys. Rev. **87**, 366 (1952).
[2] S. M. Grimes, Radiat. Eff. **94/1-4**, 995 (1986).
[3] *Proceedings of the IAEA Advisory Group on Basic and Applied Problems of Nuclear Level Densities*, edited by M. R. Bhat (BNL, Upton, New York, 1983).
[4] S. M. Grimes *et al.*, Phys. Rev. C **3**, 645 (1971).
[5] S. M. Grimes *et al.*, Phys. Rev. C **4**, 607 (1971).
[6] S. M. Grimes *et al.*, Phys. Rev. C **6**, 236 (1972).
[7] G. M. Braga-Marcazzan and L. Milazzo-Colli, Energ. Nucl. (Milan) **15**, 186 (1968).
[8] G. M. Braga-Marcazzan and L. Milazzo-Colli, Prog. Nucl. Phys. **11**, 145 (1970).
[9] J. Ernst *et al.*, Nucl. Phys. **A136**, 87 (1969).
[10] A. D. Carlson and H. H. Barschall, Phys. Rev. **158**, 1142 (1967).
[11] D. Kopsch and S. Cierjacks, in *Proceedings of the International Conference on Statistical Properties of Nuclei*, edited by J. B. Garg (Plenum, New York, 1972), p. 455.
[12] V. Mishra *et al.*, Phys. Rev. C **44**, 2419 (1991).
[13] W. Abfalterer *et al.*, Phys. Rev. C **47**, 1033 (1993).
[14] F. B. Bateman *et al.*, Phys. Rev. C **60**, 064609 (1999).
[15] T. Ericson, Phys. Rev. Lett. **5**, 430 (1960).
[16] T. Ericson, Ann. Phys. (N.Y.) **23**, 340 (1963).
[17] T. Ericson and T. Mayer Kuckuk, Annu. Rev. Nucl. Sci. **16**, 183 (1968).
[18] A. Richter, in *Nuclear Spectroscopy and Reactions*, edited by J. Cerny (Academic, New York, 1974), Pt. B, pp. 343–391.
[19] A. Agodi and C. Pappalardo, Nucl. Phys. **47**, 129 (1963).
[20] D. M. Brink and R. O. Stephen, Phys. Lett. **5**, 72 (1963).
[21] D. M. Brink *et al.*, Nucl. Phys. **54**, 577 (1964).
[22] P. A. Moldauer, Phys. Lett. **8**, 70 (1964).
[23] P. A. Moldauer, Phys. Rev. **135**, B642 (1964).
[24] P. A. Moldauer, Phys. Rev. **136**, B947 (1964).
[25] J. J. Krieger, Ann. Phys. (N.Y.) **42**, 375 (1967).
[26] M. Boehning, Annual Report Max-Planck-Institut Kernphysik, Heidelberg, 1965, pp. 106–107.
[27] P. J. Dallimore and I. Hall, Nucl. Phys. **88**, 193 (1966).
[28] J. Bardeen *et al.*, Phys. Rev. **108**, 1175 (1957).
[29] V. S. Ramamurthy, in *Proceedings of the IAEA Advisory Group on Basic and Applied Problems of Nuclear Level Densities* [3], p. 187.
[30] A. Gilbert and A. G. W. Cameron, Can. J. Phys. **43**, 1446 (1965).
[31] H. A. Bethe, Phys. Rev. **50**, 332 (1936).
[32] H. A. Bethe, Rev. Mod. Phys. **9**, 69 (1937).
[33] E. J. Burge, Nucl. Instrum. Methods **144**, 547 (1977).
[34] D. E. Bainum, Ph.D. dissertation, Ohio University, 1977.
[35] M. A. Lone, ''Cross Sections and Yields for High Energy Neutron Source Reactions,'' NBS report, 1977, p. 5.
[36] W. P. Abfalterer, Ph.D. dissertation, Ohio University, 1995.
[37] A. D. Carlson, Ph.D. thesis, University of Wisconsin, Madison, 1967.
[38] J. M. Blatt and V. F. Weisskopf, *Theoretical Nuclear Physics* (Springer-Verlag, New York, 1979), p. 389.
[39] A. C. Douglas and N. MacDonald, Nucl. Phys. **13**, 382 (1959).
[40] J. R. Huizenga *et al.*, Phys. Rev. **182**, 1149 (1969).
[41] F. S. Dietrich (private communication).
[42] J. Rapaport, V. Kulkarni, and R. W. Finlay, Nucl. Phys. **A330**, 15 (1979).
[43] F. G. Perey, Phys. Rev. **131**, 745 (1963).
[44] L. McFadden and G. R. Satchler, Nucl. Phys. **A84**, 177 (1966).
[45] S. M. Grimes, J. D. Anderson, J. W. McClure, B. A. Pohl, and C. Wong, Phys. Rev. C **10**, 2373 (1974); S. L. Graham, M. Ahmad, S. M. Grimes, H. Satyanarayana, and S. K. Saraf, Nucl. Sci. Eng. **95**, 60 (1987).
[46] L. G. Moretto, Nucl. Phys. **A182**, 641 (1972).
[47] S. G. Nilsson, K. Dan. Vidensk. Selsk., Mat. Fys. Medd. **29**, 1 (1955).
[48] P. A. Seeger and R. C. Perisho, Los Alamos Report No. LA-3751, 1967.
[49] P. A. Seeger and W. M. Howard, Nucl. Phys. **A238**, 491 (1975).
[50] N. N. Bogoliubov, Nuovo Cimento **7**, 794 (1958).
[51] G. Rohr, Z. Phys. A **318**, 299 (1984).
[52] M. Beckerman, Nucl. Phys. **A278**, 333 (1977).
[53] A. V. Ignatyuk, G. N. Smirenkin, and A. S. Tishin, Yad. Fiz. **21**, 485 (1975) [Sov. J. Nucl. Phys. **21**, 255 (1975)].
[54] A. V. Ignatyuk, K. K. Istekov, and G. N. Smirenkin, Yad. Fiz. **29**, 875 (1979) [Sov. J. Nucl. Phys. **29**, 450 (1979)].
[55] O. D. Simpson, Nucl. Instrum. Methods **30**, 293 (1964).
[56] P. W. Lisowski *et al.*, ''Nuclear Cross Sections for Technology,'' edited by J. L. Fowler, C. H. Johnson, and C. D. Bowman, NBS Special Publication No. 594, 1980, p. 524.
[57] D. C. Larson *et al.*, Report No. ORNL-TM-5612, 1976.
[58] F. G. Perey *et al.*, Report No. ORNL-TM-4823, 1972.
[59] J. D. Kellie *et al.*, J. Phys. A **5**, 1090 (1972).
[60] C. M. Perey and F. G. Perey, At. Data Nucl. Data Tables **13**, 293 (1974).
[61] D. W. Lang, Nucl. Phys. **72**, 461 (1965).
[62] S. M. Grimes, Report No. INPP-95-01, Ohio University Physics Department, 1995.
[63] A. H. Wapstra and N. B. Gove, Nucl. Data Tables **9**, 306 (1971).
[64] E. Browne *et al.*, in *Table of Isotopes*, edited by C. M. Lederer

and V. S. Shirley, 7th ed. (Wiley, New York, 1978).
[65] P. Fessenden *et al.*, Phys. Rev. Lett. **15**, 796 (1965).
[66] P. M. Endt, Nucl. Phys. **A521**, 1 (1990).
[67] D. Wilmore and P. E. Hodgson, Nucl. Phys. **55**, 673 (1964).
[68] A. B. Smith, Report No. ANL/NDM 125, 1992.
[69] A. B. Smith, Report No. ANL/NDM 120, 1991.
[70] C. Daniel and F. Wood, *Fitting Equations to Data* (Wiley-Interscience, New York, 1971).
[71] H. Vonach, in *Proceedings of the IAEA Advisory Group on Basic and Applied Problems of Nuclear Level Densities*, edited by M. R. Bhat (BNL, Upton, New York, 1983), p. 247.